RESEARCH ARTICLE

Human Mutation

OFFICIAL JOURNAL HGVS HUMAN GENOME VARIATION SOCIETY www.hgvs.org

Functional Characterization and Targeted Correction of ATM Mutations Identified in Japanese Patients with Ataxia-Telangiectasia

Kotoka Nakamura,[1] Liutao Du,[1] Rashmi Tunuguntla,[1] Francesca Fike,[1] Simona Cavalieri,[2] Tomohiro Morio,[3] Shuki Mizutani,[3] Alfredo Brusco,[2] and Richard A. Gatti[1,4]*

[1]*Department of Pathology and Laboratory Medicine, UCLA School of Medicine, Los Angeles, California;* [2]*Department of Genetics, Biology and Biochemistry, University of Torino, Medical Genetics Unit, S. Giovanni Battista Hospital, Torino, Italy;* [3]*Department of Pediatrics and Developmental Biology, Tokyo Medical and Dental University Graduate School of Medicine, Tokyo, Japan;* [4]*Department of Human Genetics, UCLA School of Medicine, Los Angeles, California*

Communicated by Michel Goossens

Received 14 June 2011; accepted revised manuscript 15 September 2011.
Published online 17 October 2011 in Wiley Online Library (www.wiley.com/humanmutation).DOI: 10.1002/humu.21632

ABSTRACT: A recent challenge for investigators studying the progressive neurological disease ataxia-telangiectasia (A-T) is to identify mutations whose effects might be alleviated by mutation-targeted therapies. We studied ATM mutations in eight families of Japanese A-T patients (JPAT) and were able to identify all 16 mutations. The probands were compound heterozygotes in seven families, and one (JPAT2) was homozygous for a frameshift mutation. All mutations—four frameshift, two nonsense, four large genomic deletions, and six affecting splicing—were novel except for c.748C>T found in family JPAT6 and c.2639-384A>G found in family JPAT11/12. Using an established lymphoblastoid cell line (LCL) of patient JPAT11, ATM protein was restored to levels approaching wild type by exposure to an antisense morpholino oligonucleotide designed to correct a pseudoexon splicing mutation. In addition, in an LCL from patient JPAT8/9, a heterozygous carrier of a nonsense mutation, ATM levels could also be partially restored by exposure to readthrough compounds (RTCs): an aminoglycoside, G418, and a novel small molecule identified in our laboratory, RTC13. Taken together, our results suggest that screening and functional characterization of the various sorts of mutations affecting the ATM gene can lead to better identification of A-T patients who are most likely to benefit from rapidly developing mutation-targeted therapeutic technologies.
Hum Mutat 33:198–208, 2012. © 2011 Wiley Periodicals, Inc.

KEY WORDS: ataxia-telangiectasia; ATM; large genomic deletions; functional analysis of DNA variants; mutation-targeted therapy; Japanese ATM mutation

Introduction

Ataxia-telangiectasia (A-T; MIM# 208900) is an autosomal recessive neurodegenerative disorder characterized by progressive cerebellar degeneration, ocular apraxia and telangiectasia, increased cancer risk, immunodeficiency, sensitivity to ionizing radiation (IR), chromosomal instability, and cell cycle abnormalities [Boder and Sedgwick, 1958; Gatti, 2001]. A-T is caused by mutations in the *ATM* gene (MIM# 607585) that usually encodes a 13 kb transcript that produces a 370 kDa protein [Gatti et al., 1988; Lange et al., 1995; Savitsky et al., 1995]. Intranuclear ATM protein is low or absent in most A-T patients, despite the presence of relatively normal levels of *ATM* transcripts. ATM is activated by autophosphorylation after binding with the MRN (Mre11-Rad50-Nbs) complex at sites of DNA double strand breaks [Bakkenist and Kastan, 2003; Kozlov et al., 2006], and subsequently phosphorylates hundreds of downstream target proteins involved in cell cycle checkpoints, DNA repair, and apoptosis [Bolderson et al., 2009; Matsuoka et al., 2007; Shiloh 2006]. ATM also appears to play a critical role in resolving chronic inflammation [Westbrook and Schiestl, 2010].

A-T patients are usually compound heterozygotes, carrying two distinct mutations. Mutations occur throughout the entire gene without hot spots. Founder effects are commonly observed in many ethnic isolates [Birrell et al., 2005; Campbell et al., 2003; Cavalieri et al., 2006; Gilad et al., 1996a; Laake et al., 1998; McConville et al., 1996; Mitui et al., 2003, 2005; Telatar et al., 1998a, b] wherein patients often carry mutations in a homozygous state. We have previously shown [Du et al., 2007, 2009, 2011; Lai et al., 2004] that accurately analyzing the functional consequences of mutations in individual A-T patients enables the grouping of patients into "mutation categories" that are most likely to be corrected by future customized mutation-targeted therapies.

The aims of the present study were to: (1) characterize the *ATM* mutations in Japanese A-T (JPAT) families; and (2) identify which JPAT patients might be candidates for personalized mutation-targeted therapy. We report that three of eight JPAT families examined are potential candidates for mutation-targeted therapy based on partial restoration of functional ATM protein production.

Materials and Methods

Cell Lines

Lymphoblastoid cell lines (LCLs) [Svedmyr et al., 1975] or activated T-cells [Minegishi et al., 2006] were established from affected

Additional Supporting Information may be found in the online version of this article.

*Correspondence to: Richard A. Gatti, Department of Pathology and Laboratory Medicine, UCLA School of Medicine, 675 Charles E. Young Drive South, Los Angeles, CA 90095-1732. E-mail: rgatti@mednet.ucla.edu

Contract grant sponsors: National Institutes of Health (1R01NS052528); A-T Ease Foundation; A-T Medical Research Foundation.

members of eight Japanese A-T families, including three sibling pairs (JPAT4/5, 8/9, and 11/12). The families came from different geographical regions. Clinical descriptions of patients from these families have been reported previously [Morio et al., 2009].

Short Tandem Repeat (STR) Haplotype Analysis

Standardized STR (short tandem repeat/microsatellite) genotyping for the *ATM* gene region was performed as previously described [Mitui et al., 2003]. Briefly, we used four fluorescently labeled microsatellite markers located within a 1.4 cM region of chromosome 11q22-q23: D11S1819, NS22, D11S2179, and D11S1818. Markers NS22 and D11S2179 are located within the *ATM* gene, in introns 45 and 62, respectively [Udar et al., 1999; Vanagaite et al., 1995]. Allelic sizes were detected with an ABI 3730 DNA analyzer (Applied Biosystems Inc, Carlsbad, CA) and standardized to a reference sample (CEPH 1347-02).

Identification of Mutations

Total RNA was isolated from patient-derived T-cell lines using RNeasy (QIAGEN, Valencia, CA), and cDNA was synthesized using random primers and the Superscript III reverse transcriptase (Invitrogen, Carlsbad, CA). The entire *ATM* coding region was divided into eight overlapping fragments (Regions 1–8) ranging from 1,500 to 1,800 bps [Du et al., 2008]. These regions were PCR amplified and then sequenced using 19 different primers. Mutations on the cDNA level were confirmed in genomic DNA (gDNA) by sequencing relevant exon and intron boundaries. Mutation analysis is based on the same ATM reference sequence used for ATM mutations in the Leiden Open Variation Database (www.LOVD.nl/ATM; NCBI reference sequence:NM_000051.3).

Maximum Entropy Scores and Search for Exonic Splicing Enhancers (ESEs)

The strength of the 5′ and 3′ splice sites (ss) was determined by calculating and comparing the wild-type and mutant 5′ and 3′ ss using the Maximum Entropy software available at http://genes.mit.edu/burgelab/maxent/Xmaxentscan_scoreseq.html [Eng et al., 2004; Mitui et al., 2009; Yeo and Burge, 2004]. We scanned for putative binding motifs for serine/arginine-rich (SR) proteins using the ESEfinder software available at http://rulai.cshl.edu/tools/ESE [Cartegni et al., 2003; Smith et al., 2006].

Long-Range PCR and Breakpoint Regions for Genomic Deletions

To amplify large gDNA fragments, 500 ng of gDNA was used as template, followed by 35 cycles of 95C for 1 min, 68°C for 10 min, and extension at 72°C for 15 min using EX Taq polymerase according to the manufacturer's protocol (Takara Bio Inc, Shiga, Japan). Fragments containing large genomic deletions (LGDs) were isolated from agarose gels and sequenced to determine the breakpoints.

Multiplex Ligation-dependent Probe Amplification (MLPA)

A total of 100 ng of gDNA was used as starting material for the SALSA MLPA P041 and P042 *ATM* kits (MRC-Holland, Amsterdam, Netherlands, www.mrc-holland.com) [Schouten et al., 2002]. The P041 probe mix contained probes for 33 of the 65 exons as well as three probes for exon 1. The P042 *ATM* probe mix contained probes for the remaining *ATM* exons. Both probe mixtures also contained probes for control genes. After hybridization, ligation, and amplification, according to the instructions of the manufacturer, 1 μl of PCR product was mixed with 0.2 μl of ROX-500 labeled internal size standard, separated on an ABI Prism 3100 Avant automatic sequencer (Applera, Norwalk, Connecticut, CA), and analyzed using the GeneScan software ver.3.1. For MLPA data analysis, we used Coffalyser MLPA DAT software developed by MRC-Holland. For each probe, a range from 1 ± 0.2 was considered as a normal exon dosage, while a deletion was determined as being between 0.3 and 0.7.

Antisense Morpholino Oligonucleotide (AMO) Design and Treatment

A 25-mer antisense morpholino oligonucleotide (AMO) was designed to target the 5′ aberrant splice site of a pseudoexon mutation in pre-mRNA of JPAT11/12. The AMO-J11 sequence was: CCTGGAAAAATACTTACAATTAAAC. AMO748C (ATTCACACACTCGAATTCGAAAGTT) and AMO4956GC (CTTGGATAACTGCAACAAATTGACA) were designed to target wild-type sequences to determine potential regulatory elements at the site of a mutation(s). AMOs were synthesized by Gene-Tools (Philomath, OR). Treatment of LCLs with AMOs was performed as previously described [Du et al., 2007]. Cells were suspended in 5% FBS/RPMI medium and the AMO was added directly to medium at the concentrations indicated. Endo-Porter (Gene-Tools) was added to the medium to assist in intracellular incorporation of the AMO. Cells were collected after 48 hr for RNA analysis, and after 84 hr for ATM protein detection. Vivo-AMO was also used to treat JPAT 11 to enhance cellular delivery (Gene-Tools).

Irradiation Induced ATM-Ser1981 Foci Formation (IRIF)

Immunostaining of nuclear foci of ATM-Ser1981was performed as described [Du et al., 2007, 2009]. In brief, LCLs were first treated with the relevant compounds for 4 days before being irradiated with 2 Gy and then incubated at 37°C for 30 min. Next, the cells were fixed with 4% paraformaldehyde and then permeabilized on cover slips. The cover slips were blocked for 1 hr and incubated with mouse anti-ATM pSer1981 for 1 hr (1:500; Cell Signaling Technology, Danvers, MA). After a second blocking, cells were stained with Alexa Fluor 488 anti-mouse IgG (1:150; Invitrogen) for 1 hr and mounted onto slides.

Flow Cytometry Analysis of ATM-Ser1981 Autophosphorylation (FC-ATM-pSer1981)

FC-ATM-pSer1981 was used to verify the restoration of Ser1981 autophosphorylation by readthrough compounds (RTCs) [Du et al., 2009; Nahas et al., 2009]. The cells were treated for 4 days with RTCs, resuspended in PBS, and irradiated with 10 Gy. After 1 hr, the cells were fixed and permeabilized using FIX & PERM (Invitrogen). The cells were then incubated with 1 μl of mouse ATM-s1981 antibody (Cell Signaling Technology) for 2 hr at room temperature. After this time, cells were washed and resuspended in 100-μl PBS with Alexa Fluor 488 anti-mouse IgG (Invitrogen) for 45 min, and then washed and resuspended in PBS with 0.2% paraformaldehyde, before being analyzed using a FACSCalibur (BD, Franklin Lakes, NJ).

Western Blotting

Nuclear extracts were prepared by following the NE-PER protocol (Thermo Fisher Scientific, Rockford, IL). Proteins were separated

on a 7.5% SDS-polyacrylamide gel. Western blots were prepared as described [Du et al., 2007], and probed with anti-ATM (Novus Biologicals, Littleton, CO), -SMC1, or -KAP1 antibodies (Novus Biologicals).

Results

Mutation Analysis

We initially screened our A-T patients for two previously reported Japanese mutations, c.4776(IVS33)+2T>A and c.7883_7887delTTATA [Ejima and Sasaki 1998; Fukao et al., 1998]. Neither of these mutations was detected.

STR genotyping of the *ATM* genomic region was performed for 11 JPAT patients, but since parental gDNAs were unavailable, we could only verify that one patient was homozygous for all markers (JPAT2): [S1819, 131; NS22, 165; S2179, 143; S1818, 162] [Mitui et al., 2003]. As a result, we set out to directly sequence the entire *ATM* coding region after PCR amplifying eight partially overlapping fragments from patients' cDNA [Du et al., 2008]. We identified 12 of the 16 expected mutations (75%) and confirmed them upon sequencing gDNA (Table 1). Only one patient (JPAT2) was homozygous, suggesting that most JPAT patients do not result from consanguineous marriages. The 12 mutations included four frameshifts (counting the homozygous JPAT2 twice), two nonsense, and six splice variants (Table 1). The remaining mutations (4/16; 25%) were four LGDs, which we identified after performing long-range PCR using gDNA as template. Fourteen mutations were novel; two had been previously reported: c.748C>T in JPAT6 [Teraoka et al., 1999] and c.2639-384A>G in JPAT11/12 [Sobeck 2001]. All mutations resulted in the absence of ATM protein (Supp. Fig. S1 and data not shown).

Splicing Mutations

The six splicing mutations identified were analyzed by using Maximum Entropy software (MaxENT) to estimate the strength of the splice sites [Yeo and Burge, 2004] and type of splice defect [Eng et al., 2004]. The mutations found are described below, and diagrams for potential splicing mechanisms are shown in Figure 1.

(1) c.331+5G>A (IVS6): This mutation changed the MaxENT score of the 5′ ss from 9.8 to 3.6. A shorter PCR product compatible with exon 6 skipping was observed at the cDNA level in patient JPAT1 using primers for exons 4 and 7 (Figs. 1 and 2A, lane 3).

(2) c.748C>T: cDNA from patient JPAT6 showed skipping of exon 9 (Figs. 1and 2B, lane 5). This allele with substitution c.748C>T predicted an amino acid change from Arg to a stop codon (CGA >TGA). Given that c.748C>T did not affect the scores for consensus splice sites, nor affect an ESE site, we hypothesized that it affected an as yet unknown splicing regulatory element. To test this idea further, we designed an AMO targeting the wild-type sequence at the site of the mutation in order to block the interaction between any regulatory molecule(s) and the wild-type sequence. Wild-type cells treated with increasing concentrations of AMO748C (Fig. 2G) showed skipping of exon 9, supporting idea model that the region around nucleotide 748 most likely contains a regulatory splicing motif.

(3) c.2639-384A>G (IVS19): The c.2639-384A>G variant in patient JPAT11/12 creates a novel splice acceptor site within IVS19 (Fig. 1), thereby creating a cryptic splice and "pseudo-exon" of 58 bp is created in intron 19 (Fig. 2C, lanes 5 and 6).

Table 1. Mutations of Eight Japanese Families

Ex/Int	Patient	cDNA change	Genomic DNA mutation	Consequence
IVS6	JPAT1[a]	c.186_331del146 (deletes exon 6)	**c.331+5G>A (5′ ss 9.81>3.58)**	Aberrant splicing (IV)
7	JPAT6[a]	c.397_398insT	**c.397_398insT**	Frameshift
9	JPAT6[b]	c.663_901del239 (deletes exon 9)	c.748C>T (R>X)	Aberrant splicing (III)
10	JPAT8/9[a]	c.902_1065del164 (deletes exon 10)	**c.902-19_1065+869del1052**	Large genomic deletion
IVS19	JPAT11/12[a]	c.2639_2640ins58	c.2639-384A>G (5′ss 0.36>8.54)	Aberrant splicing (II)
IVS19	JPAT3[a]	c.2639_2838del200 (deletes exon 20)	**c.2639-19_2639-7del13 (3′ss 8.8>3.4)**	Aberrant splicing (IV)
20	JPAT8/9[b]	c.2877C>G	**c.2877C>G (Y>X)**	Nonsense (TAG)
35	JPAT4/5[a]	c.4910_5005del96 (deletes exon 35)	**c.4956GC>TT (LQ>FX)**	Aberrant splicing (III)
38	JPAT1[b]	c.5415G>A	**c.5415G>A (W>X)**	Nonsense (TGA)
IVS48	JPAT11/12[b]	c.6808_7515del708 (deletes ex 49-52)	**c.6807+272_7516-275del5350**	Large genomic deletion
55	JPAT4/5[b]	c.7925_7926del2(GA)	**c.7925delGA**	Frameshift
60	JPAT10[a]	c.8419_8584del166 (deletes exon 60)	**c.8419-643_8507del732**	Large genomic deletion
61	JPAT10[b]	c.8585_8671del87 (deletes exon 61)	**c.8585-1G>C (5′ss 10.2>2.0)**	Aberrant splicing (IV)
61	JPAT2[b]	c.8624delA	**c.8624delA**	Frameshift
IVS63	JPAT3[b]	c.8851_9697del847	**c.8852-2kbdel17kb (CRAT [B] mutation?)**	Large genomic deletion

Bolded mutations have not been reported previously.
[a]First allele.
[b]Second allele.
[h]Homozygote.
Nucleotide numbering is based on +1 being the A of the first translation start codon in exon 4 (NCBI reference sequence: NM_000051.3).

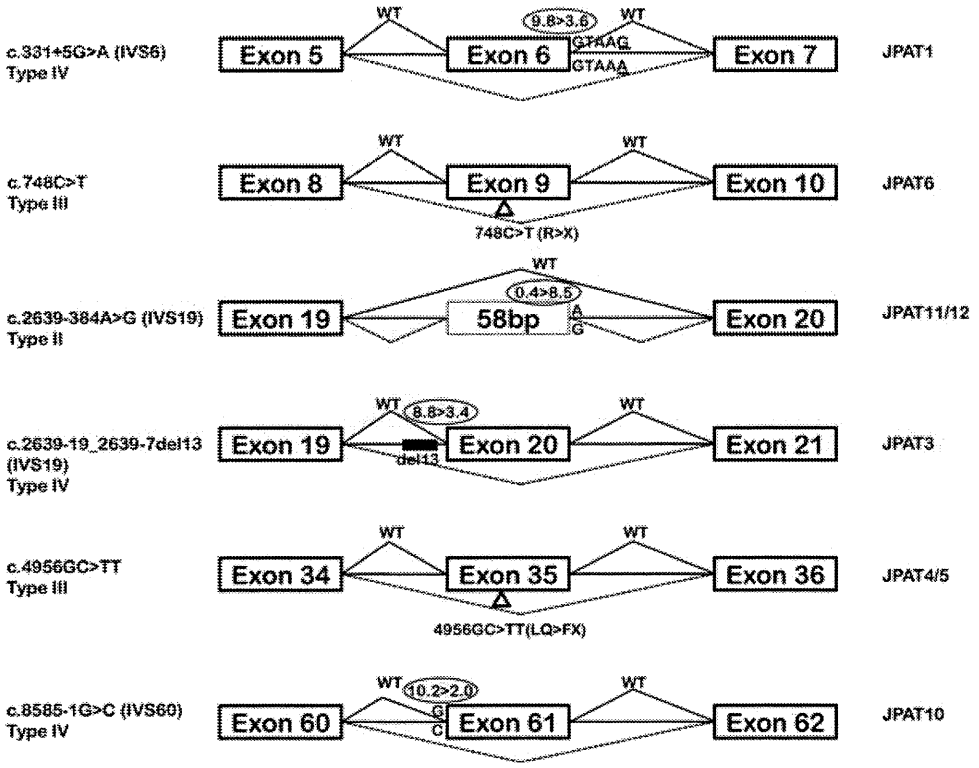

Figure 1. *ATM* splicing mutations. Genomic mutations causing splicing mutations were analyzed for changes in splicing scores calculated by Max ENT. Classification of splicing mutations is reported accordingly to Eng et al. [2004]. See text for additional details.

This results in a frameshift and a predicted secondary premature stop codon.

(4) c.2639-19_2639-7del13 (IVS19): In Figure 2D (lane 3), the PCR products from JPAT3 cDNA showed a normal and an additional prominent lower band (783 bp and 583 bp, respectively). Sequencing of the 583-bp band revealed skipping of exon 20. gDNA sequencing identified a 13 nt deletion in intron 19 at position c.2639-19_2639-7. The 3′ MaxENT score changed from 8.8 to 3.4 (Fig. 1).

(5) c.4956GC>TT: In family JPAT4/5, we identified a c.4956GC>TT substitution within exon 35 (p.LQ1652_1653FX) that leads to skipping of exon 35 without affecting an ESE or canonical splice sites (Figs. 1 and 2E, lanes 3 and 4). Exposing wild-type LCLs to increasing concentrations of AMO4956GC, targeting the mutation site, revealed skipping of exon 35 (Fig. 2H); these results suggest that nucleotide 4956 is part of a regulatory protein binding site, which when disrupted influences the aberrant splicing observed in JPAT4/5.

(6) c.8585-1G>C (IVS60): JPAT10 harbors the IVS60-1G>C mutation that changed the MaxENT score of the 3′ ss from 10.2 to 2.0, resulting in a skipping of the exon 61 (Fig. 2F, lane 4). Interestingly, the second allele of this patient was a splicing mutation that is predicted to result in exon 60 skipping (Fig. 2F, lane 4). We sequenced gDNA for exons 59–62 but failed to find a mutation that would account for the skipping of exon 60 (however, see additional results on JPAT10 below).

Large Genomic Deletions (LGDs)

(1) c.902-19_1065+869del1052 (del ex10): Two siblings (JPAT8/9) yielded an abnormal 369-bp fragment when cDNA was amplified from exon 9 to 11 (Fig. 3A, cDNA gel, lanes 3 and 4). When this band was isolated and sequenced, we found a deletion of exon 10. No mutation was observed in exons 9–11, ruling out a conventional splicing mutation. Using long-range PCR to amplify the genomic region from exon 9 to 11, we obtained a 3.3 kb fragment (Fig. 3A, gDNA gel lanes 3 and 4), whose sequence revealed a 1,052-bp deletion from IVS9-19 to IVS10+869; this deletion included exon 10 (164 bp).

(2) c.6807+272_7516-275del5350 (del ex49-52): Two siblings (JPAT11/12) showed an abnormal PCR fragment of 1.1 kb when cDNA was amplified from exon 48 to 53 (Fig. 3B, cDNA gel). The sequence of the PCR product showed a deletion of exons 49–52. A long-range PCR performed on gDNA using primers for exons 48 and 53 produced a 1.1 kb band instead of the expected 6.4 kb (Fig. 3B, left). Sequencing of the 1.1 kb band revealed a 5,350-bp genomic deletion that starts in intron 48 and ends in intron 52.

(3) c.8419-643_8507del732 (del ex 60): In patient JPAT10, we suspected that skipping of exon 60 might reflect an LGD. We amplified the gDNA surrounding exons 59–61 and found a 732-bp genomic deletion extending from IVS59-643 to nucleotide 89 of exon 60 (Fig. 3C).

(4) c.8851-2kbdel17kb (del ex64-65): When mutation screening failed to identify a second pathogenic mutation in JPAT3, we were prompted to search for an LGD mutation with Multiplex Ligation-dependent Probe Amplification (MLPA). We observed a significant decrease in peak height for the final exons 64 and 65, indicative of a deletion carried in heterozygous state (Fig. 4A). Previous studies have demonstrated two LINE-1 sequences between IVS63 and downstream of exon 65, as well as a 17 kb genomic deletion in the *ATM* gene of A-T patients

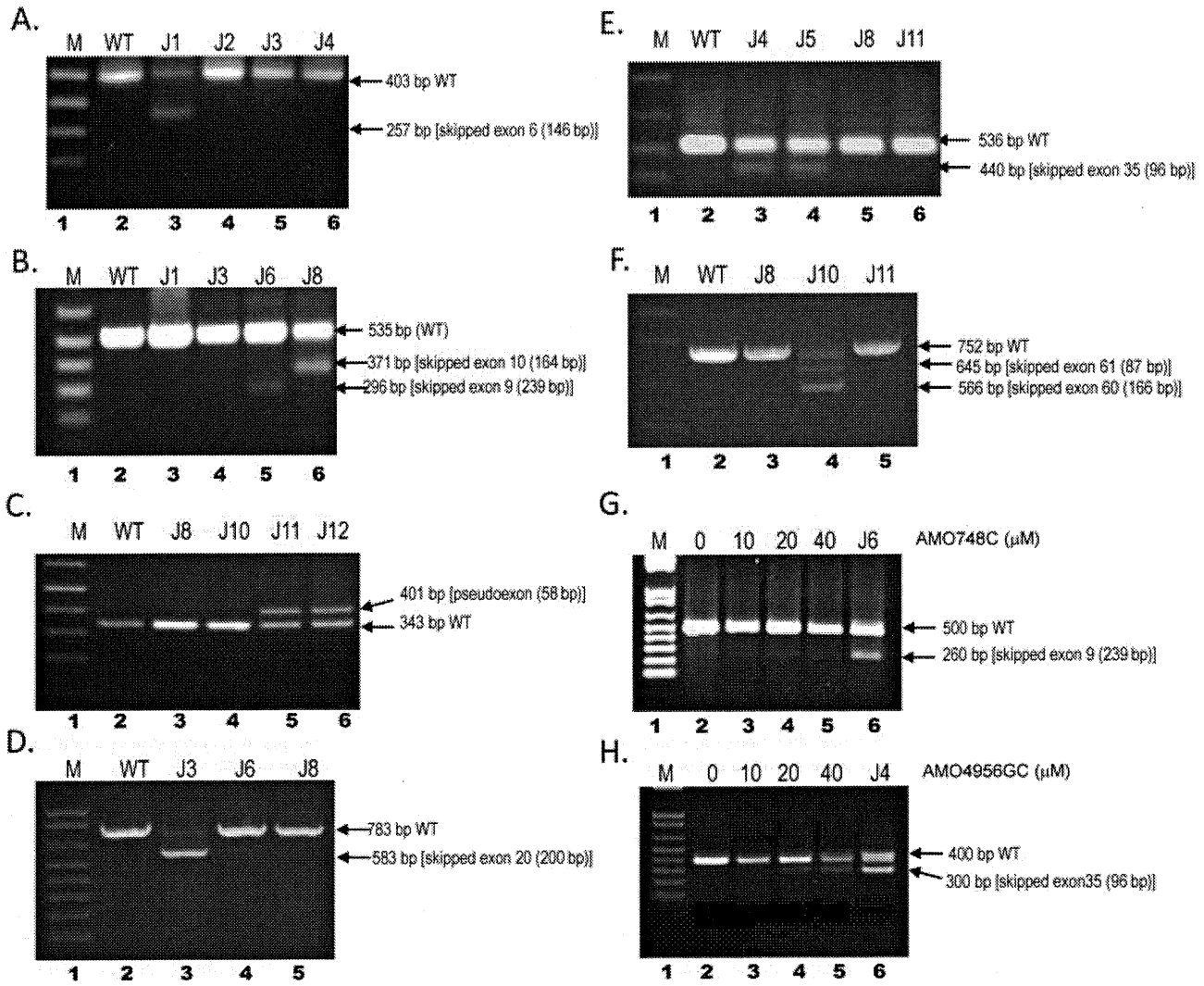

Figure 2. Effect of splicing mutations on cDNA. Agarose gel images of PCR products showed aberrant spliced products. Patient cDNA were used as templates for PCR amplifications in the regions displaying splicing mutations. M (lane 1) is 1 kb plus ladder (Invitrogen), wild-type cDNA was used as control (lane 2). **(A)** Skipped exon 6 in JPAT1 (lane 3). **(B)** Skipped exon 9 in JPAT6 (lane 5) and skipped exon 10 in JPAT8 (lane 6). **(C)** Pseudoexon of JPAT11 and JPAT12 (lanes 5 and 6). **(D)** Skipped exon 20 in JPAT3 (lane 3). **(E)** Skipped exon 35 in JPAT4 and JPAT5 (lanes 3 and 4). **(F)** Skipped exons 60 and 61 in JPAT10 (lane 4). **(G)** AMO-treated wild-type lymphoblastoid cell line (LCL) produced alternative spliced product that skipped exon 9. JPAT6, carrying the c.748C>T mutation, showed a skipped exon 9 product (lane 6), **(H)** AMO 4956GC treated wild-type LCL produced alternative spliced product that skipped exon 35. JPAT4 that has 4956GC>TT mutation showing skipped exon 35 products as a control (lane 6). See text for additional details.

with Costa Rican, Dutch, and Brazilian backgrounds [Broeks et al., 1998; Coutinho et al., 2004; Mitui et al., 2003; Telatar et al., 1998b].

Figure 4B summarizes the locations of primers, LINE-1 sequences, and an LGD for this region.

We used two sets of primers: Primer set #1 (P1Fw and P4Rev) was 23 kb apart, flanking the 17 kb deletion. Because of the nature of our PCR conditions, no PCR product was anticipated from the wild-type allele, while the mutant allele should yield a 6 kb fragment. Primer set #2 (P2Fw and P3Rev) was placed within the 17 kb deletion, which should have produced a 2.4 kb fragment from only the wild-type allele [Telatar et al., 1998b]. Figure 4B (lane 2) shows that wild-type gDNA produced the 2.4 kb fragment, while CRAT [B] (a Costa Rican patient homozygous for a 17 kb deletion) produced the 6 kb fragment (lane 4). A CRAT [B] heterozygote produced both the 2.4 kb fragment and the 6 kb product from the deletion (Fig. 4B, lane 5). The CRAT [B] band pattern was also observed in the gDNA of JPAT3, suggesting the presence of an LGD between two LINE-1 sequences (Fig. 4B, lane 3). Available breakpoints and surrounding sequences were analyzed using Repeat Masker software to search for flanking repetitive elements [Babushok and Kazazian, 2007; Kazazian and Goodier, 2002; Telatar et al., 1998b] (see Fig. 3). Because the breakpoint was in a highly homologous repeat sequence, the ends could not be accurately determined. The other Japanese patient (JPAT8) who did not have a deletion in this region showed a pattern identical to the wild type (Fig. 4B, lane 6).

The STR haplotypes for JPAT3, CRAT [B], and BRAT3 differed. JPAT3: S1819 [131,133]; NS22 [173,175]; S2179 [137,137]; S1818 [160,168]; CRAT [B]: S1819 [131]; NS22 [171]; S2179 [141]; S1818 [160] [Mitui et al., 2003]; BRAT 3: S1819 [133]; NS22 [155]; S2179

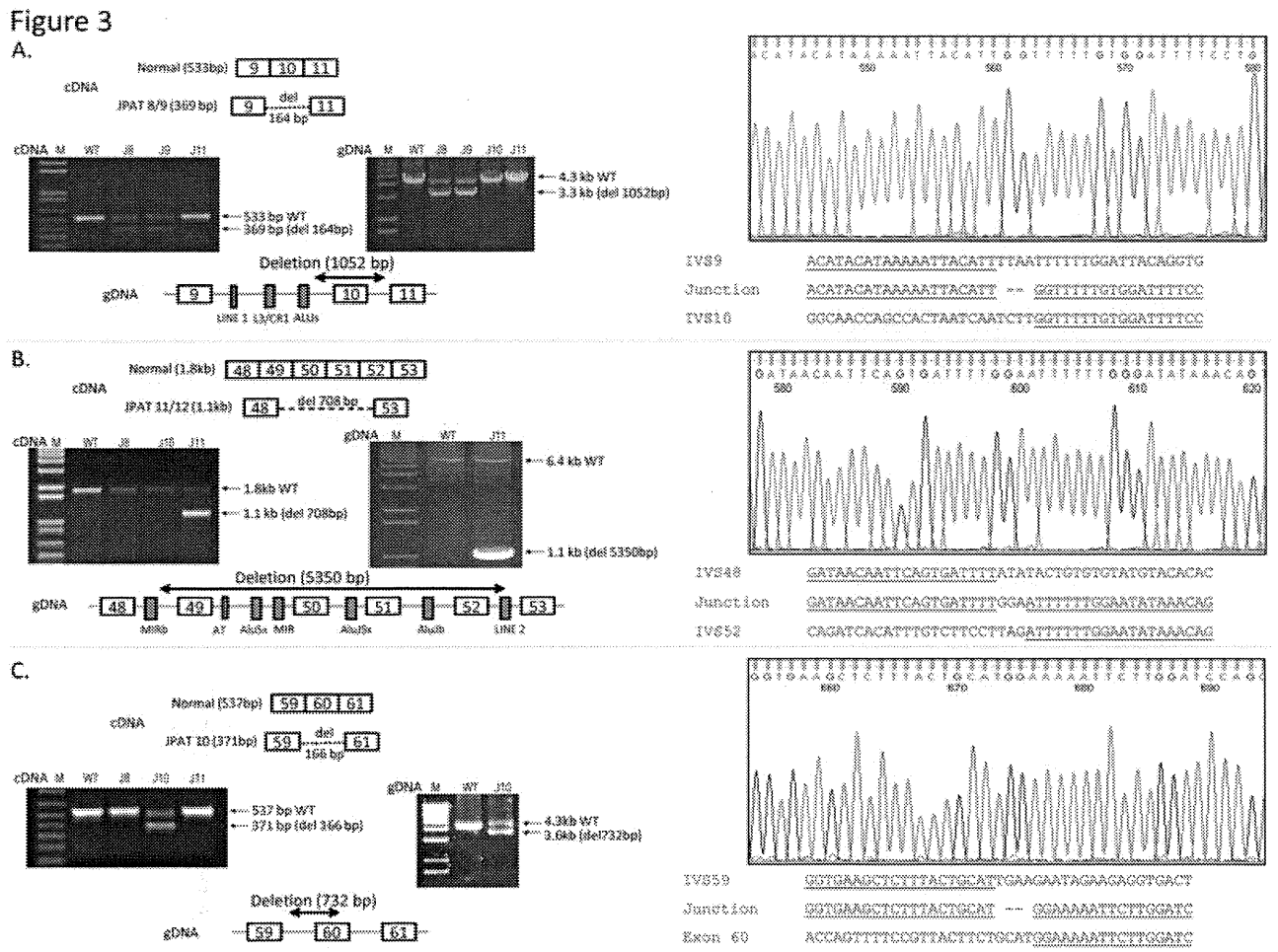

Figure 3. Large genomic deletions (LGDs). **(A)** Schematic representation of cDNA showing deletion of exon 10 and agarose gel image of PCR products (using primers GFw and GRev) (left): Lane 1 is 1 kb plus ladder (Invitrogen), lane 2 is wild-type control, lane 3 (JPAT8) and lane 4 (JPAT9) showing deletion of exon 10, lane 5 is JPAT control. Agarose gel image (right) for genomic DNA (gDNA) PCR products (using primers EX9Fw and EX11Rev) showing deletion of 1 kb in JPAT8/9. Schematic representation of DNA shows LGD, as well as repetitive elements within the region (at bottom). Sequence data with junction sequences are shown on right. **(B)** Schematic representation of cDNA change in JPAT11/12 between exon 48 and exon 53, which are analyzed by PCR (using primers FATFw and FATRev). Agarose gel image (left) for cDNA shows aberrant spliced products of JPAT11 (lane 5). Lane 1 is 1 kb plus ladder, lane 2 is wild-type, lanes 3 and 4 are JPAT control. Agarose gel image (right) for gDNA shows deletion of 5.3 kb (using EX Taq polymerase with LREX48Fw and LREX53Rev primers). Schematic representation of gDNA (at bottom) shows large deletion. Sequence data with junction sequences are shown on right. **(C)** Schematic representation of JPAT10 cDNA shows deletion of exon 60. Agarose gel image (left) shows aberrant spliced products. Agarose gel image (right) for gDNA PCR products (using primers EX59Fw and EX61Rev) show reduced size in JPAT10 (3.6 kb) compared to wild type (4.3 kb) and schematic representation of gDNA showing deletion at c.8269-643del732, which includes the first 89 bp of exon 60. Sequences are shown at right.

[147]; S1818 [146] [Mitui et al., 2003]. These results suggested that the c.8851-2kbdel17kb mutations in the three patients were not ancestrally related.

Correction of Type II Pseudoexon Splicing Mutation using an AMO

In family JPAT11/12, we identified a type II splicing mutation [Eng et al., 2004] c.2639-384A>G, which created a cryptic acceptor splice site resulting in the inclusion of 58 bp of intronic sequence (Figs. 2C and 5A). We designed AMO-J11 to target the cryptic 5′ splice site (Fig. 5A) [Du et al., 2007; Eng et al., 2004]. The LCL of JPAT11 was treated with AMO-J11 for 4 days followed by RT-PCR analysis. Mutant splicing was almost completely abrogated in an AMO dose-dependent manner and normal transcript was restored (Fig. 5B). Nuclear extracts from treated JPAT11 cells also showed a full-length ATM protein (data not shown). In order to enhance the delivery and efficiency of the AMO, we also designed a structurally modified AMO referred as "Vivo-AMO" [Morcos et al., 2008; Moulton and Jiang, 2009]. Notably, a significant amount of functional ATM protein was induced by 0.5 μM Vivo AMO-J11 (Fig. 5C). However, "Vivo-AMO" started to show possible cytotoxicity at 0.8μM (Fig. 5C, lane 4).

Correction of Nonsense Mutation in JPAT8 using RTCs

The JPAT8/9 siblings lack ATM protein because they carry an LGD and a nonsense mutation (c.2877C>G, p.Tyr959X). Functional ATM protein is inducible with compounds that readthrough premature termination codons [Du et al., 2009] even when the LCL carries the nonsense mutation in a heterozygous state [Lai et al., 2004]. We treated JPAT8 LCL with the readthrough compound RTC13 for 4

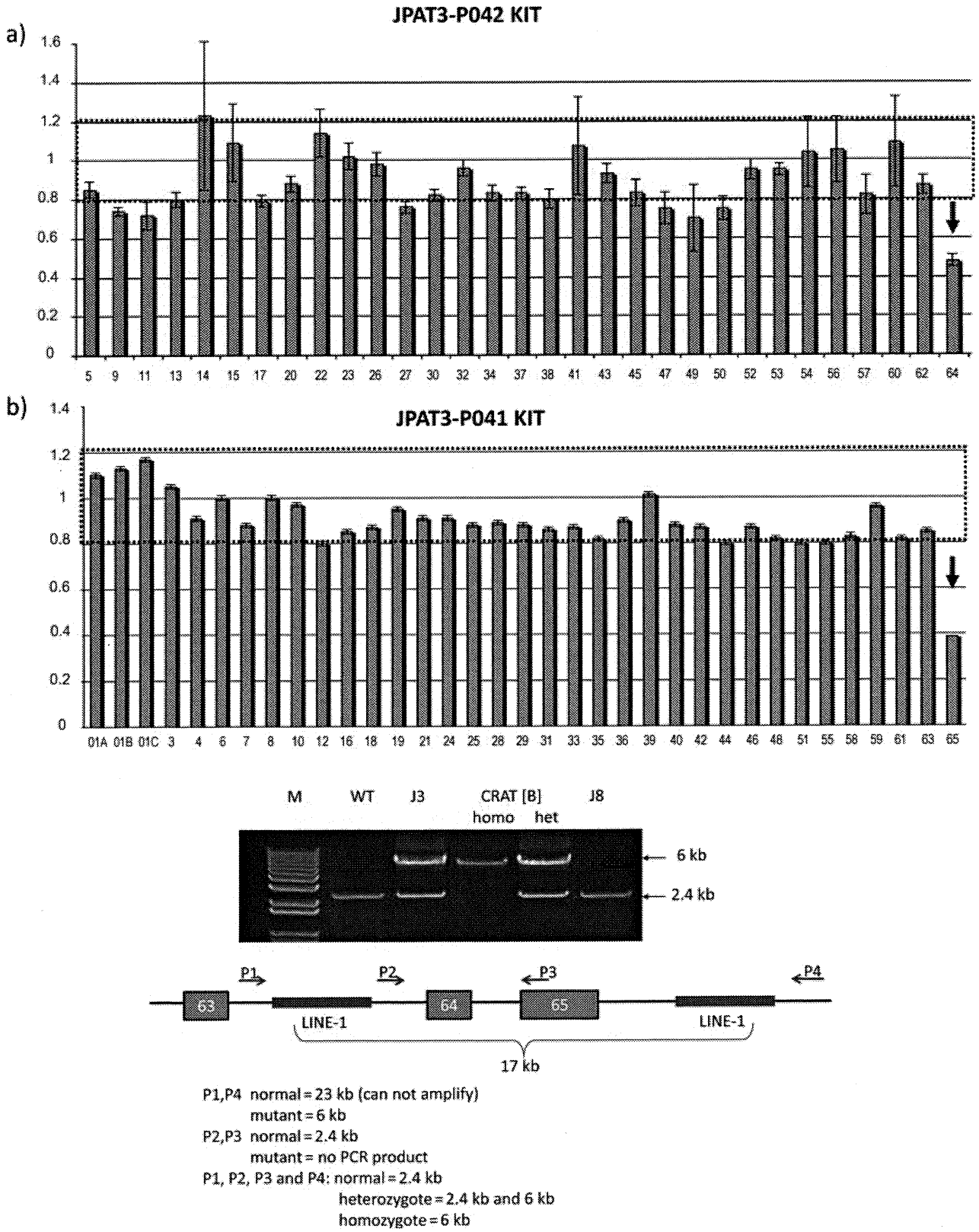

Figure 4. Analysis of LGD in patient JPAT3. **(A)** Multiplex Ligation Probe Amplification (MLPA) analysis using MLPA P041 **(A)** and P042 **(B)** kits. For each of the two analyses normalized peak area histograms of JPAT3 are shown. The dotted lines indicate the normal exon dosages between 0.8 and 1.2. The heavy black arrows indicate the exon probes of decreased signal, corresponding to the genomic deletion of exons 64 and 65. **(B)** PCR products depicting a LGD between two LINE-1 sequences. Lane 1 is 1 kb plus ladder, lane 2 is wild-type control, lane 3 is JPAT3, lane 4 is homozygous CRAT [B] patient with a very similar mutation, lane 5 is a heterozygous individual with CRAT [B] mutation, lane 6 is JPAT8. Schematic diagram (below) shows the relative locations for four different primers at the region of the LGD.

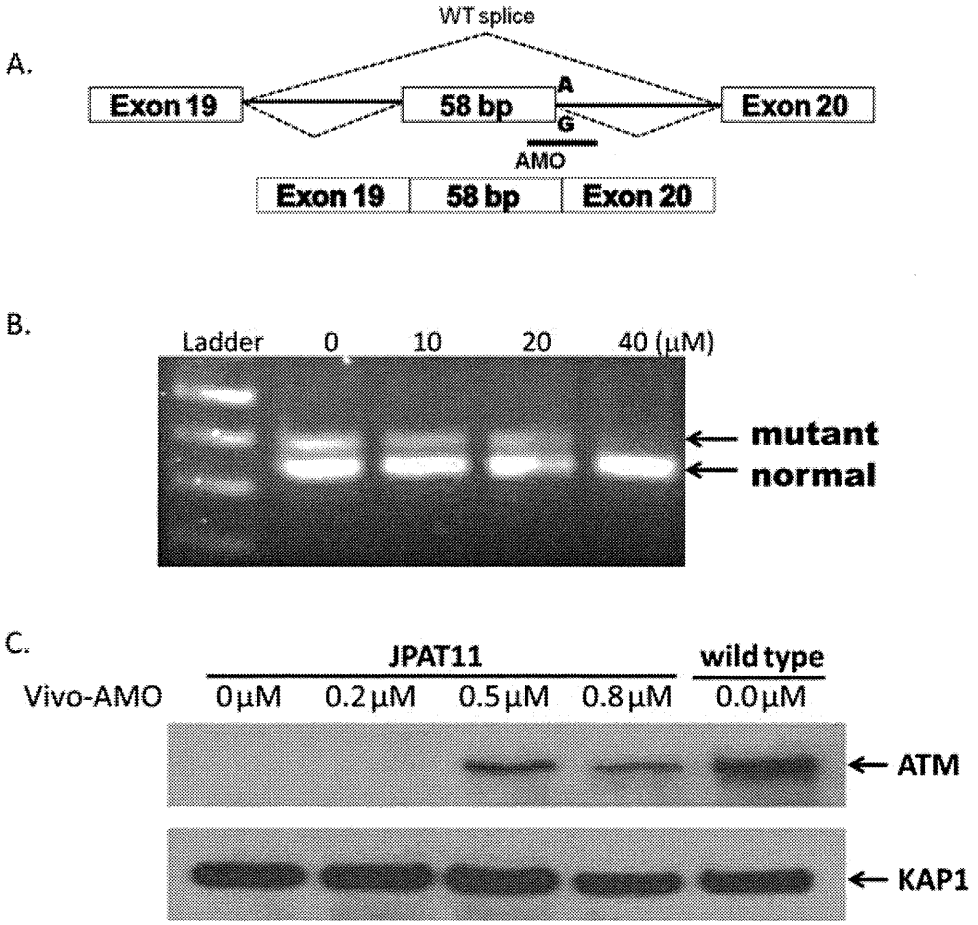

Figure 5. Correction of a splicing mutation in JPAT11 using AMO-J11. **(A)** Schematic representation of inclusion of pseudoexon (type II) and location of designed AMO. **(B)** JPAT11 cells were treated with 0, 10, 20, and 40 μM AMO for 4 days and RNAs were isolated and analyzed for corrected splicing products. **(C)** JPAT11 cells were treated with 0.2, 0.5, and 0.8 μM of Vivo-AMO-J11 for 4 days and nuclear lysates were isolated for western blotting. KAP1 antibody was used as a loading control.

days, and measured ATM autophosphorylation after DNA damage induced by IR. An aminoglycoside RTC, G418, served as a positive control. Both G418 and RTC13 successfully induced ATMpS1981 autophosphorylation as shown by (A) FC-ATMpSer1981 and (B) IRIF ATMpSer1981 assays (Fig. 6), thereby demonstrating a potential therapeutic approach for these siblings, despite the presence of a nonsense mutation in only one allele.

Discussion

Whereas a high (0.5%) coefficient of inbreeding had been recorded for the Japanese population [Pattison, 2004], the *ATM* mutation spectrum identified in our JPAT patient cohort included almost no homozygous mutations and no founder mutations. The c.4776+2T>A and c.7883_7887del5 mutations reported by Ejima and Sasaki [1998] and Fukao et al. [1998] were not observed. In fact, all mutations detected in the JPAT families—four frameshift, two nonsense, four LGDs, and six affecting splicing—were new except for a previously identified c.748C>T splicing mutation in an Irish–American family [Teraoka et al., 1999] and the c.2639-384A>G mutation [Sobeck, 2001]. It is noteworthy that only three of the six splicing mutations involved canonical sites (c.331+5G>A, c.2639-19_2639-7del13, c.8585-1G>C). In the other mutations: (1) c.748C>T (exon 9) and 4956GC>TT (exon 35) presented as nonsense mutations in gDNA, but at the cDNA level caused skipping of the exon in which they were located; and (2) JPAT11/12 had a deep-intronic mutation (c.2639-384A>G) in intron 19 that seemed to activate a cryptic acceptor splice site resulting in the insertion of a 58-bp pseudoexon in the transcript (Figs. 1, 2C, and 5).

Nonsense mutations frequently alter the splicing of the exon containing them, an observation that has been termed nonsense-associated altered splicing (NAS) [Valentine, 1998]. In most cases of NAS, the mutation disrupts an ESE critical for exon inclusion [Liu et al., 2001]. AMOs usually act by covering/masking a mutated site in the pre-mRNA, but cannot be used to correct splicing mutations at canonical sites. Thus, AMOs are most effective in correcting type II and IV splice mutations [Eng et al., 2004]. Most relevant here, AMOs can be applied to the functional analysis of *ATM* mutations. By using AMOs designed to bind the wild-type exon 9 and exon 35 sequences located around the mutation sites, we were able to induce alternative splicing (Fig. 2G and H). These results suggest that unknown regulatory elements are probably located near or at the sites of the mutation and are necessary for modulating normal splicing events in these exons. Furthermore, as described earlier, the deep-intronic mutation (c.2639-384A>G) in intron 19 is among the most attractive candidates for AMO therapy (Fig. 5) [Du et al., 2007].

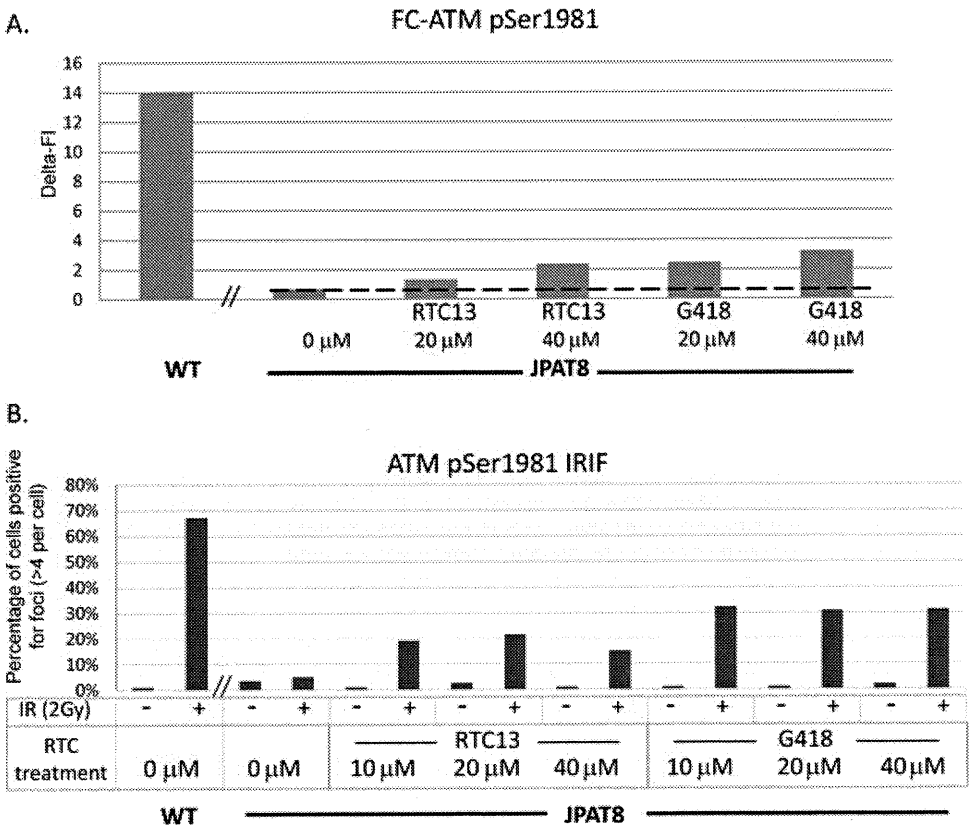

Figure 6. Readthrough compounds (RTCs) restored ATMpSer1981 autophosphorylation in JPAT8 LCL with a nonsense mutation. Cells were treated with readthrough compounds RTC13 and G418 for 4 days and then analyzed for ATMpSer1981. **(A)** ATMpSer1981 autophosphorylation level measured by FC-ATMpSer1981. Delta FI (fluorescence intensity) reflects the difference in FI between nonirradiated and irradiated cells. The data represent one of three independent experiments and results were consistent. **(B)** ATMpSer1981 foci formation by IRIF assay. The data are an average of two independent experiments.

LGDs and duplications within the *ATM* gene account for approximately 2% of reported mutations [Cavalieri et al., 2006, 2008; Coutinho, et al., 2004; Ejima and Sasaki, 1998; Gilad et al., 1996b; Mitui et al., 2003; Telatar et al., 1998b]. Few LGDs have been found in a homozygous state in A-T patients [Mitui et al., 2003]. The recent introduction of the MLPA technique has greatly improved the detection of genomic rearrangement mutations, including LGD and duplications in the *ATM* gene [Cavalieri et al., 2008].

Using MLPA, we identified the c.8851-2kbdel17kb mutation in JPAT3. While it was possible that this LGD mutation was ancestrally related to the previously reported CRAT [B] [Telatar et al., 1998a] and BRAT3 [Mitui et al., 2003] mutations, this now seems unlikely, since all three alleles are carried on different STR haplotypes. Given that homology between repetitive sequences is thought to underlie the formation of some genomic deletions and duplications [Kazazian and Goodier, 2002; Telatar et al., 1998a], we carried out an in silico analysis of DNA sequences flanking genomic deletions and were able to identify several repetitive sequences. The presence of microhomology (GGA in JPAT11) suggests that the recently described microhomology-mediated break-induced replication FoSTeS/MMBIR mechanism could be responsible for generating these deletions [Hastings et al., 2009].

Readthrough of PTCs was first described almost 50 years ago when it was noticed that certain aminoglycosides, such as streptomycin and gentamicin, "suppressed" the mutated phenotype of auxotrophy in strains of *Escherichia coli* suggesting that the drug interfered with accurate translation of the RNA code into protein [Davies et al., 1965]. Later, crystallography studies elegantly demonstrated that aminoglycosides bind to the internal loop of helix 44 (the decoding site) of the 16 S ribosomal RNA [Dibrov et al., 2010; Lynch et al., 2003]. More recently, we identified two new nonaminoglycoside small molecules with readthrough activity on both *ATM* and *dystrophin* genes [Du et al., 2009].

Based on the mutation spectrum of *ATM*, it is estimated that approximately 30% of *ATM* mutations in A-T patients are potentially treatable by mutation-targeted therapy using either RTCs or AMOs. This includes A-T patients who are compound heterozygotes, since RTCs and AMOs restore significant amounts of ATM protein even when only one allele is targeted. We identified three such examples amongst the eight Japanese families. In fact, in vitro, we were able to correct (1) abnormal splicing for JPAT11/12 (Fig. 5A), using a custom-designed AMO to mask the cryptic splice site created by the pseudoexon mutation (c.2639-384A>G); (2) a nonsense mutation in cells from JPAT8/9 using RTCs (Fig. 6). Thus, our results demonstrate that mutation-targeted treatment of cells carrying poorly understood DNA variants can extend our understanding of the consequences of such changes and may also have important therapeutic potential.

Acknowledgments

S.C. received a fellowship from "Associazione Gli Amici di Valentina." We thank Drs. Shareef Nahas, Hailiang Hu, and Mark Ambrose for helpful discussions.

References

Babushok DV, Kazazian HH, Jr. 2007. Progress in understanding the biology of the human mutagen LINE-1. Hum Mutat 28:527–539.

Bakkenist CJ, Kastan MB. 2003. DNA damage activates ATM through intermolecular autophosphorylation and dimer dissociation. Nature 421:499–506.

Birrell GW, Kneebone K, Nefedov M, Nefedova E, Jartsev MN, Mitsui M, Gatti RA, Lavin MF. 2005. ATM mutations, haplotype analysis, and immunological status of Russian patients with ataxia telangiectasia. Hum Mutat 25:593–601.

Boder E, Sedgwick RP. 1958. Ataxia-telangiectasia; a familial syndrome of progressive cerebellar ataxia, oculocutaneous telangiectasia and frequent pulmonary infection. Pediatrics 21:526–554.

Bolderson E, Richard DJ, Zhou BB, Khanna KK. 2009. Recent advances in cancer therapy targeting proteins involved in DNA double-strand break repair. Clin Cancer Res 15:6314–6320.

Broeks A, de Klein A, Floore AN, Muijtjens M, Kleijer WJ, Jaspers NG, van 't Veer LJ. 1998. ATM germline mutations in classical ataxia-telangiectasia patients in the Dutch population. Hum Mutat 12:330–337.

Campbell C, Mitui M, Eng L, Coutinho G, Thorstenson Y, Gatti RA. 2003. ATM mutations on distinct SNP and STR haplotypes in ataxia-telangiectasia patients of differing ethnicities reveal ancestral founder effects. Hum Mutat 21:80–85.

Cartegni L, Wang J, Zhu Z, Zhang MQ, Krainer AR. 2003. ESEfinder: a web resource to identify exonic splicing enhancers. Nucleic Acids Res 31:3568–3571.

Cavalieri S, Funaro A, Pappi P, Migone N, Gatti RA, Brusco A. 2008. Large genomic mutations within the ATM gene detected by MLPA, including a duplication of 41 kb from exon 4 to 20. Ann Hum Genet 72(Pt 1):10–18.

Cavalieri S, Funaro A, Porcedda P, Turinetto V, Migone N, Gatti RA, Brusco A. 2006. ATM mutations in Italian families with ataxia telangiectasia include two distinct large genomic deletions. Hum Mutat 27:1061–1070.

Coutinho G, Mitui M, Campbell C, Costa Carvalho BT, Nahas S, Sun X, Huo Y, Lai CH, Thorstenson Y, Tanouye R, Raskin S, Kim CA, Llerena J Jr, Gatti RA. 2004. Five haplotypes account for fifty-five percent of ATM mutations in Brazilian patients with ataxia telangiectasia: seven new mutations. Am J Med Genet A 126:33–40.

Davies J, Gorini L, Davis BD. 1965. Misreading of RNA codewords induced by aminoglycoside antibiotics. Mol Pharmacol 1:93–106.

Dibrov SM, Parsons J, Hermann T. 2010. A model for the study of ligand binding to the ribosomal RNA helix h44. Nucleic Acids Res 38:4458–4465.

Du L, Damoiseaux R, Nahas S, Gao K, Hu H, Pollard JM, Goldstine J, Jung ME, Henning SM, Bertoni C, Gatti RA. 2009. Nonaminoglycoside compounds induce readthrough of nonsense mutations. J Exp Med 206:2285–2297.

Du L, Kayali R, Bertoni C, Fike F, Hu H, Iversen PL, Gatti RA. 2011. Arginine-rich cell-penetrating peptide dramatically enhances AMO-mediated ATM aberrant splicing correction and enables delivery to brain and cerebellum. Hum Mol Genet 20:3151–3160.

Du L, Lai CH, Concannon P, Gatti RA. 2008. Rapid screen for truncating ATM mutations by PTT-ELISA. Mutat Res 640:139–144.

Du L, Pollard JM, Gatti RA. 2007. Correction of prototypic ATM splicing mutations and aberrant ATM function with antisense morpholino oligonucleotides. Proc Natl Acad Sci USA 104:6007–6012.

Ejima Y, Sasaki MS. 1998. Mutations of the ATM gene detected in Japanese ataxia-telangiectasia patients: possible preponderance of the two founder mutations 4612del165 and 7883del5. Hum Genet 102:403–408.

Eng L, Coutinho G, Nahas S, Yeo G, Tanouye R, Babaei M, Dork T, Burge C, Gatti RA. 2004. Nonclassical splicing mutations in the coding and noncoding regions of the ATM Gene: maximum entropy estimates of splice junction strengths. Hum Mutat 23:67–76.

Fukao T, Song XQ, Yoshida T, Tashita H, Kaneko H, Teramoto T, Inoue R, Katamura K, Mayumi M, Hiratani M and others. 1998. Ataxia-telangiectasia in the Japanese population: identification of R1917X, W2491R, R2909G, IVS33+2T->A, and 7883del5, the latter two being relatively common mutations. Hum Mutat 12:338–343.

Gatti RA. 2001. Ataxia-telangiectasia. In: Scriver CR, Beaudet AL, Sly WS, Valle D, editors. The Metabolic and Molecular Basis of Inherited Disease. Edition 8. New York: McGraw-Hill 677–704.

Gatti RA, Berkel I, Boder E, Braedt G, Charmley P, Concannon P, Ersoy F, Foroud T, Jaspers NG, Lange K and others. 1988. Localization of an ataxia-telangiectasia gene to chromosome 11q22–23. Nature 336:577–580.

Gilad S, Bar-Shira A, Harnik R, Shkedy D, Ziv Y, Khosravi R, Brown K, Vanagaite L, Xu G, Frydman M, and others. 1996a. Ataxia-telangiectasia: founder effect among north African Jews. Hum Mol Genet 5:2033–2037.

Gilad S, Khosravi R, Shkedy D, Uziel T, Ziv Y, Savitsky K, Rotman G, Smith S, Chessa L, Jorgensen TJ and others. 1996b. Predominance of null mutations in ataxia-telangiectasia. Hum Mol Genet 5:433–439.

Hastings PJ, Ira G, Lupski JR. 2009. A microhomology-mediated break-induced replication model for the origin of human copy number variation. PLoS Genet 5:e1000327.

Kazazian HH, Jr., Goodier JL. 2002. LINE drive. Retrotransposition and genome instability. Cell 110:277–280.

Kozlov SV, Graham ME, Peng C, Chen P, Robinson PJ, Lavin MF. 2006. Involvement of novel autophosphorylation sites in ATM activation. EMBO J 25:3504–3514.

Laake K, Telatar M, Geitvik GA, Hansen RO, Heiberg A, Andresen AM, Gatti R, Borresen-Dale AL. 1998. Identical mutation in 55% of the ATM alleles in 11 Norwegian AT families: evidence for a founder effect. Eur J Hum Genet 6:235–244.

Lai CH, Chun HH, Nahas SA, Mitui M, Gamo KM, Du L, Gatti RA. 2004. Correction of ATM gene function by aminoglycoside-induced read-through of premature termination codons. Proc Natl Acad Sci USA 101:15676–15681.

Lange E, Borresen AL, Chen X, Chessa L, Chiplunkar S, Concannon P, Dandekar S, Gerken S, Lange K, Liang T and others. 1995. Localization of an ataxia-telangiectasia gene to an approximately 500-kb interval on chromosome 11q23.1: linkage analysis of 176 families by an international consortium. Am J Hum Genet 57:112–119.

Liu HX, Cartegni L, Zhang MQ, Krainer AR. 2001. A mechanism for exon skipping caused by nonsense or missense mutations in BRCA1 and other genes. Nat Genet 27:55–58.

Lynch SR, Gonzalez RL, Puglisi JD. 2003. Comparison of X-ray crystal structure of the 30S subunit-antibiotic complex with NMR structure of decoding site oligonucleotide-paromomycin complex. Structure 11:43–53.

Matsuoka S, Ballif BA, Smogorzewska A, McDonald ER, 3rd, Hurov KE, Luo J, Bakalarski CE, Zhao Z, Solimini N, Lerenthal Y and others. 2007. ATM and ATR substrate analysis reveals extensive protein networks responsive to DNA damage. Science 316:1160–1166.

McConville CM, Stankovic T, Byrd PJ, McGuire GM, Yao QY, Lennox GG, Taylor MR. 1996. Mutations associated with variant phenotypes in ataxia-telangiectasia. Am J Hum Genet 59:320–330.

Minegishi Y, Saito M, Morio T, Watanabe K, Agematsu K, Tsuchiya S, Takada H, Hara T, Kawamura N, Ariga T and others. 2006. Human tyrosine kinase 2 deficiency reveals its requisite roles in multiple cytokine signals involved in innate and acquired immunity. Immunity 25:745–755.

Mitui M, Bernatowska E, Pietrucha B, Piotrowska-Jastrzebska J, Eng L, Nahas S, Teraoka S, Sholty G, Purayidom A, Concannon P and others. 2005. ATM gene founder haplotypes and associated mutations in Polish families with ataxia-telangiectasia. Ann Hum Genet 69(Pt 6):657–664.

Mitui M, Campbell C, Coutinho G, Sun X, Lai CH, Thorstenson Y, Castellvi-Bel S, Fernandez L, Monros E, Carvalho BT and others. 2003. Independent mutational events are rare in the ATM gene: haplotype prescreening enhances mutation detection rate. Hum Mutat 22:43–50.

Mitui M, Nahas SA, Du LT, Yang Z, Lai CH, Nakamura K, Arroyo S, Scott S, Purayidom A, Concannon P and others. 2009. Functional and computational assessment of missense variants in the ataxia-telangiectasia mutated (ATM) gene: mutations with increased cancer risk. Hum Mutat 30:12–21.

Morcos PA, Li Y, Jiang S. 2008. Vivo-Morpholinos: a non-peptide transporter delivers Morpholinos into a wide array of mouse tissues. Biotechniques 45:613–614, 616, 618 passim.

Morio T, Takahashi N, Watanabe F, Honda F, Sato M, Takagi M, Imadome K, Miyawaki T, Delia D, Nakamura K and others. 2009. Phenotypic variations between affected siblings with ataxia-telangiectasia: ataxia-telangiectasia in Japan. Int J Hematol 90:455–462.

Moulton JD, Jiang S. 2009. Gene knockdowns in adult animals: PPMOs and vivomorpholinos. Molecules 14:1304–1323.

Nahas SA, Butch AW, Du L, Gatti RA. 2009. Rapid flow cytometry-based structural maintenance of chromosomes 1 (SMC1) phosphorylation assay for identification of ataxia-telangiectasia homozygotes and heterozygotes. Clin Chem 55:463–472.

Pattison JE. 2004. A comparison of inbreeding rates in India, Japan, Europe and China. HOMO—J Comp Hum Biol 55:113–128.

Savitsky K, Bar-Shira A, Gilad S, Rotman G, Ziv Y, Vanagaite L, Tagle DA, Smith S, Uziel T, Sfez S and others. 1995. A single ataxia telangiectasia gene with a product similar to PI-3 kinase. Science 268:1749–1753.

Schouten JP, McElgunn CJ, Waaijer R, Zwijnenburg D, Diepvens F, Pals G. 2002. Relative quantification of 40 nucleic acid sequences by multiplex ligation-dependent probe amplification. Nucleic Acids Res 30:e57.

Shiloh Y. 2006. The ATM-mediated DNA-damage response: taking shape. Trends Biochem Sci 31:402–410.

Smith PJ, Zhang C, Wang J, Chew SL, Zhang MQ, Krainer AR. 2006. An increased specificity score matrix for the prediction of SF2/ASF-specific exonic splicing enhancers. Hum Mol Genet 15:2490–2508.

Sobeck A. 2001. Caretaker-Gen-Syndrome:Molekulargenetische und Funktionelle Studien. PhD Thesis, Wuerzburg: Julius-Maximilians-University Wuerzburg.

Svedmyr EA, Leibold W, Gatti RA. 1975. Possible use of established cell lines for MLR locus typing. Tissue Antigens 5:186–195.

Telatar M, Teraoka S, Wang Z, Chun HH, Liang T, Castellvi-Bel S, Udar N, Borresen-Dale AL, Chessa L, Bernatowska-Matuszkiewicz E and others. 1998a. Ataxia-telangiectasia: identification and detection of founder-effect mutations in the ATM gene in ethnic populations. Am J Hum Genet 62:86–97.

Telatar M, Wang S, Castellvi-Bel S, Tai LQ, Sheikhavandi S, Regueiro JR, Porras O, Gatti RA. 1998b. A model for ATM heterozygote identification in a large population: four founder-effect ATM mutations identify most of Costa Rican patients with ataxia telangiectasia. Mol Genet Metab 64:36–43.

Teraoka SN, Telatar M, Becker-Catania S, Liang T, Onengut S, Tolun A, Chessa L, Sanal O, Bernatowska E, Gatti RA and others. 1999. Splicing defects in the ataxia-telangiectasia gene, ATM: underlying mutations and consequences. Am J Hum Genet 64:1617–1631.

Udar N, Farzad S, Tai LQ, Bay JO, Gatti RA. 1999. NS22: a highly polymorphic complex microsatellite marker within the ATM gene. Am J Med Genet 82:287–289.

Valentine CR. 1998. The association of nonsense codons with exon skipping. Mutat Res 411:87–117.

Vanagaite L, James MR, Rotman G, Savitsky K, Bar-Shira A, Gilad S, Ziv Y, Uchenik V, Sartiel A, Collins FS and others. 1995. A high-density microsatellite map of the ataxia-telangiectasia locus. Hum Genet 95:451–454.

Westbrook AM, Schiestl RH. 2010. Atm-deficient mice exhibit increased sensitivity to dextran sulfate sodium-induced colitis characterized by elevated DNA damage and persistent immune activation. Cancer Res 70:1875–1884.

Yeo G, Burge CB. 2004. Maximum entropy modeling of short sequence motifs with applications to RNA splicing signals. J Comput Biol 11:377–394.

of departure from Hardy–Weinberg equilibrium ($P=0.06$), because the variant G allele is significantly more prevalent among Whites than non-Whites with the allele frequency of 0.24 versus 0.073, respectively ($P=0.0003$). Still, the observed associations retained significance in analyses restricted only to Whites. The G allele was associated with better EFS and OS in univariate analyses ($P=0.0173$ and 0.035, respectively, data not shown) and in multivariable analyses ($P=0.023$ and 0.005, respectively, data not shown).

We also observed that the variant A allele of FKBP5 SNP rs7755289 (T>A; intron 8) was significantly associated with worse EFS ($P=0.014$, hazard ratio = 3.193, 95% CI = 1.258–8.104, Figure 1c) and OS ($P=0.0036$, hazard ratio = 4.846, 95% CI = 1.68–14, Figure 1d). In addition, A allele was associated with increased day 22 MRD ($P=0.017$), increased cumulative incidence of relapse ($P=0.045$, hazard ratio = 3.4, 95% CI = 1.03–11.22) and an increased cumulative incidence of treatment-related mortality ($P=0.012$, hazard ratio = 5.57, 95% CI = 1.44–21.47). However, as this SNP occurred with the allele frequency of only ~0.2, the low sample size restricted us from performing further analysis. Although the above mentioned SNPs were the most interesting SNPs, we also observed association of SNP rs16878591 ($P=0.011$) with day 22 MRD levels and SNPs within LD block-2 with *in vitro* ara-C LC_{50} values ($P=0.03$; Table 1).

In previous reports, FKBP5 expression has been shown to positively influence response to cytarabine and gemcitabine. More recently, FKBP5 has been identified as scaffolding protein that facilitates PHLPP-mediated dephosphorylation of AKT-Ser473, thus indicating that higher expression of FKBP5 might contribute to enhanced chemosensitivity.[3–5] siRNA-mediated FKBP5 knockdown increases the resistance to cytarabine and other agents as etoposide, paclitaxel and doxetaxel.[1,3–5] Thus, FKBP5 SNPs may also be associated with response to other agents used in combination with cytarabine in AML patients. In conclusion, our preliminary results suggest that the FKBP5 polymorphisms mentioned above may also be relevant for AML treatment response. These results should be confirmed with functional studies and independent clinical studies. Identification of pharmacogenetic markers of response, such as FKBP5 SNP such as rs3798346, might help in further understanding inter-patient variation in response to chemotherapy.

Conflict of interest

The authors declare no conflict of interest.

Acknowledgements

We acknowledge the support from NIH R01CA132946 (LAMBA) and the Cancer Center Support (CORE) P30 CA021765 grants from the National Institutes of Health, and by the American Lebanese Syrian Associated Charities. Help from Biomedical genomics center, University of Minnesota in performing genotyping is highly appreciated.

AK Mitra[1], K Crews[2], S Pounds[3], X Cao[3], JR Downing[4], S Raimondi[4], D Campana[5], RC Ribeiro[5], JE Rubnitz[5] and JK Lamba[1]

[1]*Department of Experimental and Clinical Pharmacology, University of Minnesota, Minneapolis, MN, USA;*
[2]*Department of Pharmaceutical Sciences, St Jude Children's Research Hospital, Memphis, TN, USA;*
[3]*Department of Biostatistics, St Jude Children's Research Hospital, Memphis, TN, USA;*
[4]*Department of Pathology, St Jude Children's Research Hospital, Memphis, TN, USA and*
[5]*Department of Oncology, St Jude Children's Research Hospital, Memphis, TN, USA*
E-mail: lamba004@umn.edu

References

1 Li L, Fridley B, Kalari K, Jenkins G, Batzler A, Safgren S *et al.* Gemcitabine and cytosine arabinoside cytotoxicity: association with lymphoblastoid cell expression. *Cancer Res* 2008; **68**: 7050–7058.
2 Jinwal UK, Koren III J, Borysov SI, Schmid AB, Abisambra JF, Blair LJ *et al.* The Hsp90 cochaperone, FKBP51, increases Tau stability and polymerizes microtubules. *J Neurosci* 2010; **30**: 591–599.
3 Li L, Lou Z, Wang L. The role of FKBP5 in cancer aetiology and chemoresistance. *Br J Cancer* 2011; **104**: 19–23.
4 Pei H, Li L, Fridley BL, Jenkins GD, Kalari KR, Lingle W *et al.* FKBP51 affects cancer cell response to chemotherapy by negatively regulating Akt. *Cancer Cell* 2009; **16**: 259–266.
5 Pei H, Lou Z, Wang L. Emerging role of FKBP51 in AKT kinase/protein kinase B signaling. *Cell Cycle* 2010; **9**: 6–7.
6 Rubnitz JE, Inaba H, Dahl G, Ribeiro RC, Bowman WP, Taub J *et al.* Minimal residual disease-directed therapy for childhood acute myeloid leukaemia: results of the AML02 multicentre trial. *Lancet Oncol* 2010; **11**: 543–552.
7 Lamba JK, Crews K, Pounds SB, Cao X, Gandhi V, Plunkett W *et al.* Identification of predictive markers of cytarabine response in acute myeloid leukemia by integrative analysis of gene-expression profiles with multiple phenotypes. *Pharmacogenomics* 2011; **12**: 327–239.
8 Benjamini YaH, Hochberg Y. Controlling the false discovery rate: a practical and powerful approach to multiple testing. *J Royal Stat Soc* 1995. Series B. **57**: 289–300.

CBL mutation in childhood therapy-related leukemia

Leukemia (2011) **25**, 1356–1358; doi:10.1038/leu.2011.75; published online 15 April 2011

Therapy-related leukemia and myelodysplastic syndrome (t-Leuk/MDS) are mainly caused by topoisomerase II inhibitors that cause acute myeloid leukemia (AML) with an 11q23 translocation or by alkylating agents that induce MDS/AML with an *AML1* mutation and monosomy 7.[1,2] Two types of t-Leuk/MDS can be distinguished, one of which has a long latency (≥5–7 years) and is seen following alkylating agents, frequently with an preleukemic phase.[1] The other has a short latency period (1–3 years), no preleukemic phase, and is strongly associated with the administration of topoisomerase II inhibitors and chromosomal abnormalities involving 11q23 translocation/*MLL* rearrangement (*MLL*-R).[2] Repair of etoposide (VP-16)-stabilized DNA topoisomerase II covalent complexes may initiate *MLL*-R observed in patients.[3]

In this regard, recent reports of somatic mutations of the *CBL* proto-oncogene in myeloid neoplasms are intriguing, because

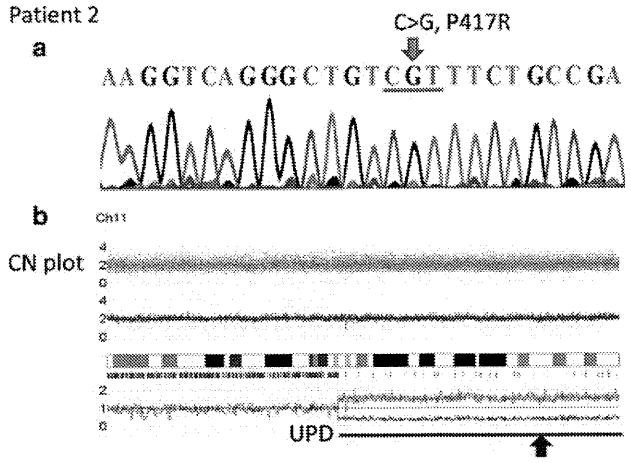

Figure 1 Identification of acquired isodisomy of 11q and *CBL* mutation in therapy-related leukemia. (**a**) Homozygous mutation of the *CBL* gene was identified in patient 2. (**b**) Copy number (CN) analysis for the gene chip output for therapy-related leukemia in patient 2. Total CNs (red plot) are shown above the cytoband, and the result of allele-specific CN analysis with anonymous references plots are shown below the cytoband. Larger allele is presented in red line, and smaller allele is presented in green line. Allele-specific analysis showed 11q-aUPD (blue line), which contained *CBL* region (black arrow).

these *CBL* mutations were shown to result in aberrant tyrosine kinase signaling, which would lead also to activation of RAS signaling pathways. We and others reported that *CBL* mutations occurred in a variety of myeloid neoplasms, including *de novo* AML,[4] MDS[4] and myeloproliferative neoplasm,[4,5] especially in chronic myelomonocytic leukemia[5] and juvenile myelomonocytic leukemia.[6] The importance of *CBL* mutations concerning about leukemogenesis is substantially increased. This prompted us to search for possible *CBL* mutations in pediatric t-Leuk/MDS.

Analysis of *CBL* gene was carried out in 20 pediatric t-Leuk/MDSs, including 15 AMLs (range: 1 year and 10 months to 17 years; 8 males and 7 females), 4 MDSs (range: 7 years to 14 years; 4 males) and 1 acute lymphoblastic leukemia (4 years and 2 months; 1 male). Median age at diagnosis was 8 years and 1 months (range: 1 year and 10 months to 17 years; 13 males and 7 females). Rearrangements of *MLL* gene were found in 17 patients (85%), including 15 of 16 who received VP-16 (Sugita *et al.*[7]), and 2 of 4 who did not receive it. An initial diagnosis was made as non-Hodgkin's lymphoma in seven patients, neuroblastoma in five, acute lymphoblastic leukemia in five, AML in two and juvenile myelomonocytic leukemia in one.

Because *CBL* mutations thus far reported almost exclusively involved exons 8–9 that encode linker/RING finger domains,[4–6] we confined our mutation analysis to these exons, in which PCR-amplified exons 8–9 were subjected to direct sequencing using an ABI PRISM 310 Genetic Analyzer (Applied Biosystems, Branchburg, NJ, USA). The study adhered to the principles of the Helsinki declaration, and was conducted under the regulations enacted by the Ethics Board of Gunma Children's Medical Center.

Homozygous mutation of the *CBL* gene was identified in 1 out of the 20 t-Leuk/MDS cases (5%), which were located in the RING finger domain (P417R in patient 2). As the frequency of 11q-acquired uniparental disomy (11q-aUPD) was reported ~85–90% in *CBL* mutations,[4–6] we analyzed his sample using Affymetrix GeneChip 250K *Nsp*I array (Affymetrix, Santa Clara, CA, USA), and found the presence of 11q-aUPD, which was the sole abnormality seen by single-nucleotide polymorphism array (Figure 1), confirming a strong association of *CBL* mutations with 11q-aUPD as previously described.[4–6] Furthermore, we examined *NRAS* and *KRAS* mutations in these patients whose samples were available and found *KRAS* mutation in one patient with t-Leuk (acute monocytic leukemia having t(9;11)(p21;q23) after B-cell precursor acute lymphoblastic leukemia having 6p−, 7q+, 9q+ and 12q−).

CBL mutation was detected in MDS cells from the patient with t-MDS after malignant lymphoma. The patient was initially diagnosed as having diffuse large T-cell type malignant lymphoma, whose biopsied specimen of the buccal lymph node showed MT1(+), MB1(−) and UCHL1(+), when he was 5 years old. He subsequently was treated with chemotherapy according to T-8801 protocol including VP-16 (200 mg/m^2) given twice weekly,[7] and obtained a complete remission. However, at 7 months after diagnosis, tumor appeared in the right maxilla, and was diagnosed as the relapsed lymphoma, then, he received local irradiation (30 Gy) and chemotherapy including ifosfamide, vincristine, THP-adriamycin and L-asparaginase. At 4 months later, enlarged spleen was resected, and the infiltrated tumor cells were microscopically seen in the tumor sections. At 6 months later, 19 months after initial diagnosis, blast cells appeared in peripheral blood. His laboratory data revealed leukocytosis (14 700/μl with 18% blast cells) and an elevated serum lactate dehydrogenase level (1458 U/l). Bone marrow aspiration revealed 9.8% blasts, which were positive for cytoplasmic myeloperoxidase, suggesting MDS. Surface marker analysis showed that the leukemic blasts in the bone marrow were positive for CD33. Chromosomal analysis of bone marrow cells revealed t(5;11)(q21;q23) in 11 of 20 cells. Rearrangement of *MLL* gene of these cells was identified by Southern blotting, however, no known chimeric mRNA with *MLL*, such as *MLL-AF5q31* and *MLL-GRAF* in t(5;11)(q31;q23), could be detected. These suggested that the gene at 5q21 was a novel partner gene of *MLL*. Although another chemotherapy for AML was performed, his blast cells increased >30% blasts in bone marrow at 25 months after initial diagnosis. Therefore, he was diagnosed as having t-Leuk resembling acute monoblastic leukemia due to VP-16. He died of mycotic infection at 35 months after initial diagnosis.

No *CBL* mutations were found in his lymphoma sample at diagnosis and in tumor cells in the enlarged spleen. We also performed tissue-fluorescence *in situ* hybridization analysis with *MLL* probe on paraffin-embedded tissue sections of the tumor cells in the enlarged spleen, however, no evaluable results could be detected because of poor quality of samples. No initial samples for tissue-fluorescence *in situ* hybridization analysis could be obtained.

The 11q23 translocation/*MLL*-R in t-Leuk/MDS was considered to be induced by VP-16,[3] however, gene alterations in addition to *MLL*-R have rarely reported. Recently, *CBL* mutations were found in a variety of myeloid neoplasms.[4–6] Among 2000 samples from the patients with myeloid neoplasms, *CBL* mutations have been found in ~5% samples, including AML transformed from MDS, but not *de novo* or therapy-related acute leukemia with 11q23 translocation/*MLL*-R. To our knowledge, this is the first t-Leuk/MDS patient with 11q23 translocation/*MLL*-R and *CBL* mutation. Interestingly, a *de novo* AML case with *MLL–CBL* fusion gene has also been reported.[8] These findings suggest that alterations of *CBL* gene and 11q23 translocation/*MLL*-R may cooperate in the pathogenesis of a subtype of t-Leuk/MDS and *de novo* leukemia.

Conflict of interest

The authors declare no conflict of interest.

Acknowledgements

We thank Mrs Chisato Murata and Miss Sayaka Takeuchi, for their excellent technical assistance. This work was supported by a grant for Cancer Research, a grant for Research on Children and Families, and Research on intractable diseases, Health and Labor Sciences Research Grants from the Ministry of Health, Labor, and Welfare of Japan, a Grant-in-Aid for Scientific Research (B, C) and Exploratory Research from the Ministry of Education, Culture, Sports, Science, and Technology of Japan and by a Research grant for Gunma Prefectural Hospitals.

N Shiba[1,2], T Taki[3], M-j Park[1], M Nagasawa[4], T Kanazawa[2], J Takita[5], H Ohnishi[6], M Sotomatsu[1], H Arakawa[2] and Y Hayashi[1]
[1]Department of Hematology/Oncology, Gunma Children's Medical Center, Shibukawa, Japan;
[2]Department of Pediatrics, Gunma University Graduate School of Medicine, Maebashi, Japan;
[3]Department of Molecular Diagnostics and Therapeutics, Kyoto Prefectural University of Medicine Graduate School of Medical Science, Kyoto, Japan;
[4]Department of Developmental Biology, Post Graduate School, Tokyo Medical and Dental University, Tokyo, Japan;
[5]Department of Pediatrics, Graduate School of Medicine, University of Tokyo, Tokyo, Japan and
[6]Department of Laboratory Medicine, Kyorin University School of Medicine, Tokyo, Japan
E-mail: hayashiy-tky@umin.ac.jp

References

1 Tucker MA, Meadows AT, Boice Jr JD, Stovall M, Oberlin O, Stone BJ *et al.* Leukemia after therapy with alkylating agents for childhood cancer. *J Natl Cancer Inst* 1987; **78**: 459–464.
2 Pui CH, Ribeiro RC, Hancock ML, Rivera GK, Evans WE, Raimondi SC *et al.* Acute myeloid leukemias in children treated with epipodophyllotoxins for acute lymphoblastic leukemia. *N Engl J Med* 1991; **325**: 1682–1687.
3 Nakada S, Katsuki Y, Imoto I, Yokoyama T, Nagasawa M, Inazawa J *et al.* Early G2/M checkpoint failure as a molecular mechanism underlying etoposide-induced chromosomal aberrations. *J Clin Invest* 2006; **116**: 80–89.
4 Grand FH, Hidalgo-Curtis CE, Ernst T, Zoi K, Zoi C, McGuire C *et al.* Frequent CBL mutations associated with 11q acquired uniparental disomy in myeloproliferative neoplasms. *Blood* 2009; **113**: 6182–6192.
5 Sanada M, Suzuki T, Shih LY, Otsu M, Kato M, Yamazaki S *et al.* Gain-of-function of mutated C-CBL tumour suppressor in myeloid neoplasms. *Nature* 2009; **460**: 904–908.
6 Shiba N, Kato M, Park MJ, Sanada M, Ito E, Fukushima K *et al.* CBL mutations in juvenile myelomonocytic leukemia and pediatric myelodysplastic syndrome. *Leukemia* 2010; **24**: 1090–1092.
7 Sugita K, Furukawa T, Tsuchida M, Okawa Y, Nakazawa S, Akatsuka J *et al.* High frequency of etoposide (VP-16)-related secondary leukemia in children with non-Hodgkin's lymphoma. *Am J Pediatr Hematol Oncol* 1993; **15**: 99–104.
8 Fu JF, Hsu JJ, Tang TC, Shih LY. Identification of CBL, a proto-oncogene at 11q23.3, as a novel MLL fusion partner in a patient with *de novo* acute myeloid leukemia. *Genes Chromosomes Cancer* 2003; **37**: 214–219.

SNP array analysis of leukemic relapse samples after allogeneic hematopoietic stem cell transplantation with a sibling donor identifies meiotic recombination spots and reveals possible correlation with the breakpoints of acquired genetic aberrations

Leukemia (2011) **25**, 1358–1361; doi:10.1038/leu.2011.79; published online 15 April 2011

Allogeneic hematopoietic stem cell transplantation (HSCT) with a sibling donor is commonly used for treating hematologic malignancies.[1] Although this procedure is frequently curative, a proportion of the patients eventually suffers a relapse of the original malignancy.[1] Leukemogenesis is associated with acquired genetic aberrations caused by various mechanisms including induction of double-stranded DNA breaks by DNA toposiomerase II poisons followed by non-homologous end joining, recombination between homologous sequences and illegitimate V(D)J recombination.[2] It has been hypothesized that neoplasia-associated breakpoints may correlate with the breakpoints of meiotic events, that is, some parts of the genome are more prone to both meiotic and somatic rearrangements; however, this remains controversial.[3–5]

During the last five years, numerous studies have used single-nucleotide polymorphism (SNP) array analysis to investigate genetic abnormalities in hematologic malignancies, including paired diagnostic and relapse samples.[6] To the best of our knowledge, however, the particular scenario of a relapse occurring after allogeneic HSCT with a sibling donor has not been addressed with this technique. In such cases, the bone marrow consists of a mixture of the patient-derived leukemic cells and the donor-derived normal hematopoietic cells, displaying different degrees of chimerism depending on the proportion of leukemic cells. In the present study, we have investigated hematologic malignancies that relapsed after allogeneic HSCT with a sibling donor, and we here provide examples and discuss the particular properties of these samples in terms of SNP array analysis. Furthermore, we have, for the first time, investigated whether the breakpoints of acquired leukemia-associated genetic abnormalities and meiotic recombination events are correlated in a single individual genome.

The study included six cases of relapsed hematologic malignancies after HSCT with a sibling donor, comprising one acute myeloid leukemia M0, two acute myeloid leukemia M5, two myelodysplastic syndromes and one chronic myeloid leukemia. DNA was extracted according to standard methods from bone marrow samples obtained at relapse. In addition, a dilution series of a mixture of peripheral blood samples from two unrelated healthy individuals was prepared in ratios of 1:9, 2:8, 3:7, 4:6 and 5:5. SNP array analysis was performed using the Illumina 1M-duo bead Infinium BD BeadChip platform (Illumina, San Diego, CA, USA) as previously described.[7] Expected B-allele frequency (BAF) values for each combination of genotypes in two mixed cell populations were calculated using the formula $BAF_{exp} = [B_1p + B_2(1-p)]/[L_1p + L_2(1-p)]$, where B is the number of B alleles in the respective cell population, p is the frequency of cell population 1, and L is the

DNMT3A mutations are rare in childhood acute myeloid leukaemia, myelodysplastic syndromes and juvenile myelomonocytic leukaemia

Acute myeloid leukaemia (AML) is a complex disease caused by mutations and deregulated gene expression, leading to increased proliferation and decreased differentiation of haematopoietic progenitor cells. Contemporary treatments have resulted in 5-year event-free survival rates of almost 60% for paediatric AML (Pui *et al*, 2011).

Recently, a whole genome sequencing study of AML uncovered recurrent mutations of an epigenetic regulator, the *DNA methyltransferase 3A* (*DNMT3A*) gene, in approximately 20% of adult AML patients (Ley *et al*, 2010; Yamashita *et al*, 2010; Yan *et al*, 2011). In these studies, *DNMT3A* mutations were frequently associated with *FLT3*-internal tandem duplication (ITD), *nucleophosmin 1* (*NPM1*) and *isocitrate dehydrogenase 1* (*IDH1*) mutations (Ley *et al*, 2010; Yan *et al*, 2011). *DNMT3A* mutations were also found in adult myelodysplastic syndromes (MDS) (8%, 12/150) (Walter *et al*, 2011), AML secondary to myeloproliferative neoplasms (MPNs) (14%, 5/35), myelofibrosis (15%, 3/20) and polycythaemia vera (7%, 2/30) (Stegelmann *et al*, 2011).

DNMT3A is involved in epigenetic regulation of genes by enzymatic de novo addition of methyl groups to the cytosine residue of CpG dinucleotides. *DNMT3A* mutations were significantly enriched with a cytogenetic profile associated with intermediate risk, including a normal cytogenetic profile, as well as the M4 and M5 subtypes, according to the French-American-British (FAB) classification system (Ley *et al*, 2010; Yan *et al*, 2011). In AML patients with a normal karyotype and *FLT3*-ITD, patients with *DNMT3A* gene mutations showed a worse prognosis than those without *DNMT3A* gene mutations (Ley *et al*, 2010; Yan *et al*, 2011); however, the frequency and clinical impact of *DNMT3A* gene mutations in paediatric AML and myeloproliferative neoplasms (MPN) remain uncertain. We searched for *DNMT3A* gene mutations in 149 AMLs who were treated on the Japanese Childhood AML Cooperative protocol, AML 99 (range: 0–15 years old, M0: 5, M1: 23, M2: 44, M3: 13, M4: 22, M5: 21, M6: 1, M7: 17, unclassified: three patients), 40 juvenile myelomonocytic leukaemias (JMMLs; range: 2 months to 8 years), 24 myelodysplastic syndromes (MDSs) and 20 paediatric therapy-related leukaemia/MDSs (t-Leuk/MDSs, range: 1–17 years). *FLT3*-ITD and *NPM1* gene alterations have been reported in these 149 AML patients (Shimada *et al*, 2007, 2008).

Total RNA extracted from the bone marrow or peripheral blood samples at diagnosis was reverse transcribed to cDNA with a cDNA Synthesis Kit (Amersham Bioscience, Tokyo, Japan). *DNMT3A* mutations were thus far reported to be almost exclusively involved in exons 16-23 (especially codon R882 in exon 23) (Ley *et al*, 2010; Yamashita *et al*, 2010; Stegelmann *et al*, 2011; Walter *et al*, 2011; Yan *et al*, 2011); thus, we confined our analysis to these exons. cDNA was amplified using the following primers: *DNMT3A* cDNA 15F, 5′-CAGGTGCTTTTGCGTGGAGTGT-3′ and 19R, 5′-ATGC AGGAGGCGGTAGAACTCA-3′, 17F, 5′-AAGATCATGTAC-GTCGGGGA-3′ and 22R, 5′-CTTTGCCCTGCTTTA TG-GAG-3′ and 20F, 5′-CCCTGTGATGATTGATGCCA-3′ and 23R, 5′-GTATTTCCGCCTCTGTG-GTT-3′ for AML samples. For JMML, MDS and t-Leuk/MDS, we confined our analysis to exon 23, including the hotspot of codon R882, of the *DNMT3A* gene using the following primers: *DNMT3A* DNA 23F, 5′-AGAACTAAGCAGGGCC-TCAGAGGA-3′ and 23R, 5′-GTATTTCCGCCTCTGTGGTT-3′. Subsequently, direct sequencing was performed on a DNA sequencer (ABI 310; Applied Biosystems, Foster City, CA, USA) using a BigDye terminator cycle sequencing kit (Applied Biosystems). The study adhered to the principles of the Helsinki Declaration, and was conducted under the regulations enacted by the Ethics Board of Gunma Children's Medical Centre.

No *DNMT3A* mutations were detected in any AML patients in our study. Recently, *DNMT3A* mutations have been reported in paediatric AML patients (Ho *et al*, 2011; Thol *et al*, 2011). Only two patients were identified (both 15 years old). Combined with these and our data, the frequency of *DNMT3A* mutations is extremely rare (2/524, 0·4%) in childhood AML. Furthermore, we did not identify *DNMT3A* mutations in MDS, JMML or paediatric t-Leuk/MDS. These findings were not compatible with those of adult MDS and MPN, suggesting that the frequency of *DNMT3A* gene mutations depends on age.

On the other hand, we found *FLT3*-ITD in 20 (13%) of 149 AML patients; however, no *NPM1* mutations were found (Shimada *et al*, 2007, 2008). Nine AML patients with *FLT3*-ITD were found to lack *DNMT3A* mutation. *DNMT3A* mutations have been correlated with *FLT3*-ITD and *NPM1* in adult AML, but not in paediatric AML. Although patients with *DNMT3A* mutations have been associated with FAB-M4, M5, especially *MLL*-negative M5, no mutations in these paediatric M4/M5 patients were found in this study. *DNMT3A* mutations have not been detected in any adult AML with favourable cytogenetics, including *t*(8;21) and inv(16) (Ley *et al*, 2010; Yan *et al*, 2011). Higher frequencies of *t*(8;21) and inv(16) in

paediatric than in adult AML patients may be associated with rare *DNMT3A* mutations in paediatric AML. These data suggest that the pathology of paediatric AML may be different from that of adult AML. We concluded that *DNMT3A* mutations, as well as *NPM1* mutations, may be infrequent in paediatric AML and MDS patients, especially those <15 years old.

Acknowledgements

We thank Mrs. Chisato Murata for her excellent technical assistance. This work was supported by a grant for Cancer Research, a grant for Research on Children and Families, and Research on Intractable Diseases, Health and Labour Sciences Research Grants from the Ministry of Health, Labour, and Welfare of Japan, a Grant-in-Aid for Scientific Research (B, C) and Exploratory Research from the Ministry of Education, Culture, Sports, Science, and Technology of Japan and by a Research grant for Gunma Prefectural Hospitals.

Authorship

TT and YH designed the study. AS, MS, SA, AT, KH and MT provided critical reagents and samples. NS and MP performed the experiments. RH, IT and HA supervised the work. NS and MP analysed the results. NS, TT, and YH wrote the paper and all the authors critically reviewed and revised it.

Conflict of interest

The authors declare no conflicts of interest.

Norio Shiba[1,2]
Tomohiko Taki[3]
Myoung-ja Park[1]
Akira Shimada[4]
Manabu Sotomatsu[1]
Souichi Adachi[5]
Akio Tawa[6]
Keizo Horibe[7]
Masahiro Tsuchida[8]
Ryoji Hanada[9]
Ichiro Tsukimoto[10]
Hirokazu Arakawa[2]
Yasuhide Hayashi[1]

[1]Department of Haematology/Oncology, Gunma Children's Medical Centre, Shibukawa, [2]Department of Paediatrics, Gunma University Graduate School of Medicine, Maebashi, [3]Department of Molecular Diagnostics and Therapeutics, Kyoto Prefectural University of Medicine Graduate School of Medical Science, Kyoto, [4]Department of Paediatrics, Nagoya University Graduate School of Medicine, Nagoya, [5]Department of Human Health Sciences, Kyoto University Graduate School of Medicine, Kyoto, [6]Department of Paediatrics, National Hospital Organization Osaka National Hospital, Osaka, [7]Clinical Research Centre, National Hospital Organization Nagoya Medical Centre, Nagoya, [8]Department of Paediatrics, Ibaraki Children's Hospital, Ibaraki, [9]Division of Haematology/Oncology, Saitama Children's Medical Centre, Saitama, and [10]Department of First Peadiatrics, Toho University School of Medicine, Tokyo, Japan.
E-mail: hayashiy-tky@umin.ac.jp

Keywords: AML, myeloproliferative neoplasms, paediatric, *DNMT3A*.

First published online 8 October 2011
doi: 10.1111/j.1365-2141.2011.08879.x

References

Ho, P.A., Kutny, M.A., Alonzo, T.A., Gerbing, R.B., Joaquin, J., Raimondi, S.C., Gamis, A.S. & Meshinchi, S. (2011) Leukemic mutations in the methylation-associated genes DNMT3A and IDH2 are rare events in pediatric AML: a report from the Children's Oncology Group. *Pediatric Blood & Cancer*, **57**, 204–209.

Ley, T.J., Ding, L., Walter, M.J., McLellan, M.D., Lamprecht, T., Larson, D.E., Kandoth, C., Payton, J.E., Baty, J., Welch, J., Harris, C.C., Lichti, C.F., Townsend, R.R., Fulton, R.S., Dooling, D.J., Koboldt, D.C., Schmidt, H., Zhang, Q., Osborne, J.R., Lin, L., O'Laughlin, M., McMichael, J.F., Delehaunty, K.D., McGrath, S.D., Fulton, L.A., Magrini, V.J., Vickery, T.L., Hundal, J., Cook, L.L., Conyers, J.J., Swift, G.W., Reed, J.P., Alldredge, P.A., Wylie, T., Walker, J., Kalicki, J., Watson, M.A., Heath, S., Shannon, W.D., Varghese, N., Nagarajan, R., Westervelt, P., Tomasson, M.H., Link, D.C., Graubert, T.A., DiPersio, J.F., Mardis, E.R. & Wilson, R.K. (2010) DNMT3A mutations in acute myeloid leukemia. *New England Journal of Medicine*, **363**, 2424–2433.

Pui, C.H., Carroll, W.L., Meshinchi, S. & Arceci, R.J. (2011) Biology, risk stratification, and therapy of pediatric acute leukemias: an update. *Journal of Clinical Oncology*, **29**, 551–565.

Shimada, A., Taki, T., Kubota, C., Tawa, A., Horibe, K., Tsuchida, M., Hanada, R., Tsukimoto, I. & Hayashi, Y. (2007) No nucleophosmin mutations in pediatric acute myeloid leukemia with normal karyotype: a study of the Japanese Childhood AML Cooperative Study Group. *Leukemia*, **21**, 1307.

Shimada, A., Taki, T., Tabuchi, K., Taketani, T., Hanada, R., Tawa, A., Tsuchida, M., Horibe, K., Tsukimoto, I. & Hayashi, Y. (2008) Tandem duplications of MLL and FLT3 are correlated with poor prognoses in pediatric acute myeloid leukemia: a study of the Japanese childhood AML Cooperative Study Group. *Pediatric Blood & Cancer*, **50**, 264–269.

Stegelmann, F., Bullinger, L., Schlenk, R.F., Paschka, P., Griesshammer, M., Blersch, C., Kuhn, S., Schauer, S., Döhner, H. & Döhner, K. (2011) DNMT3A mutations in myeloproliferative neoplasms. *Leukemia*, **25**, 1217–1219.

Thol, F., Heuser, M., Damm, F., Klusmann, J.H., Reinhardt, K. & Reinhardt, D. (2011) DNMT3A mutations are rare in childhood acute myeloid leukemia. *Haematologica*, **96**, 1238–1240.

Walter, M.J., Ding, L., Shen, D., Shao, J., Grillot, M., McLellan, M., Fulton, R., Schmidt, H., Kalicki-Veizer, J., O'Laughlin, M., Kandoth, C., Baty, J., Westervelt, P., Dipersio, J.F., Mardis, E.R., Wilson, R.K., Ley, T.J. & Graubert, T.A. (2011) Recurrent DNMT3A mutations in patients with myelodysplastic syndromes. *Leukemia*, **25**, 1153–1158.

Yamashita, Y., Yuan, J., Suetake, I., Suzuki, H., Ishikawa, Y., Choi, Y.L., Ueno, T., Soda, M., Hamada, T., Haruta, H., Takada, S., Miyazaki, Y., Kiyoi, H., Ito, E., Naoe, T., Tomonaga, M., Toyota, M., Tajima, S., Iwama, A. & Mano, H. (2010) Array-based genomic resequencing of human leukemia. *Oncogene*, **29**, 3723–3731.

Yan, X.J., Xu, J., Gu, Z.H., Pan, C.M., Lu, G., Shen, Y., Shi, J.Y., Zhu, Y.M., Tang, L., Zhang, X.W., Liang, W.X., Mi, J.Q., Song, H.D., Li, K.Q., Chen, Z. & Chen, S.J. (2011) Exome sequencing identifies somatic mutations of DNA methyltransferase gene DNMT3A in acute monocytic leukemia. *Nature Genetics*, **43**, 309–315.

Brief report

Heterozygous *ITGA2B* R995W mutation inducing constitutive activation of the αIIbβ3 receptor affects proplatelet formation and causes congenital macrothrombocytopenia

Shinji Kunishima,[1] Hirokazu Kashiwagi,[2] Makoto Otsu,[3] Naoya Takayama,[3] Koji Eto,[3] Masafumi Onodera,[4] Yuji Miyajima,[5] Yasushi Takamatsu,[6] Junji Suzumiya,[7] Kousaku Matsubara,[8] Yoshiaki Tomiyama,[2,9] and Hidehiko Saito[10]

[1]Department of Advanced Diagnosis, Clinical Research Center, National Hospital Organization Nagoya Medical Center, Nagoya, Japan; [2]Department of Hematology and Oncology, Graduate School of Medicine, Osaka University, Osaka, Japan; [3]Division of Stem Cell Therapy, Center for Stem Cell and Regenerative Medicine, Institute of Medical Science, University of Tokyo, Tokyo, Japan; [4]Department of Genetics, National Research Institute for Child Health and Development, Tokyo, Japan; [5]Department of Pediatrics, Anjo Kosei Hospital, Anjo, Japan; [6]Department of Medical Oncology, Hematology and Infectious Disease, Fukuoka University, Fukuoka, Japan; [7]Shimane University Hospital Cancer Center, Shimane, Japan; [8]Department of Pediatrics, Nishi-Kobe Medical Center, Kobe, Japan; [9]Department of Blood Transfusion, Osaka University Hospital, Osaka, Japan; and [10]Nagoya Central Hospital, Nagoya, Japan

Congenital macrothrombocytopenia is a genetically heterogeneous group of rare disorders. αIIbβ3 has not been implicated in these conditions. We identified a novel, conserved heterozygous *ITGA2B* R995W mutation in 4 unrelated families. The surface expression of platelet αIIbβ3 was decreased to 50% to 70% of control. There was spontaneous PAC-1 and fibrinogen binding to resting platelets without CD62p expression. The activation state of αIIbβ3 in 293T cells was higher for αIIb-W995 than for β3-H723 but was weaker than for β3-N562. FAK was spontaneously phosphorylated in αIIb-W995/β3-transfected 293T cells. These results indicate that αIIb-W995/β3 has a constitutive, activated conformation but does not induce platelet activation. αIIb-W995/β3-transfected CHO cells developed membrane ruffling and abnormal cytoplasmic protrusions. The increased size and decreased number of proplatelet tips in αIIb-W995/β3-transduced mouse fetal liver-derived megakaryocytes indicate defective proplatelet formation. We propose that activating mutations in *ITGA2B* and *ITGB3* represent the etiology of a subset of congenital macrothrombocytopenias. (*Blood.* 2011;117(20):5479-5484)

Introduction

Congenital macrothrombocytopenia is a genetically heterogeneous group of rare disorders.[1-4] The most frequent forms include *MYH9* disorders and Bernard-Soulier syndrome. In approximately half of cases of congenital macrothrombocytopenia, the pathogenesis remains unknown; thus, a definite diagnosis is unavailable. Glanzmann thrombasthenia is the most common congenital platelet disorder caused by qualitative or quantitative abnormality of the integrin αIIbβ3, in which the platelet counts and morphology are normal.[5] However, *ITGA2B* R995Q mutation has been reported in a patient with Glanzmann thrombasthenia-like phenotype and macrothrombocytopenia.[6,7] Recently, heterozygous *ITGB3* mutations were found in patients with congenital macrothrombocytopenia.[8-10] We report here a novel, conserved heterozygous *ITGA2B* R995W mutation in 4 unrelated families.

Methods

Patients

Twenty-seven patients with congenital macrothrombocytopenia, in whom *MYH9* disorders, heterozygous and homozygous Bernard-Soulier syndrome, type 2B von Willebrand disease, and *TUBB1* mutations were excluded, underwent mutational analysis of *ITGA2B* and *ITGB3*. Fifty-five consecutive patients were prospectively analyzed for the surface expression of platelet αIIbβ3. Written informed consent was obtained from all patients or their parents in accordance with the Declaration of Helsinki. Institutional review boards of Nagoya Medical Center and each of the participating institutions/hospitals approved this study.

Genetic analysis

The entire coding sequence of exons and exon-intron boundaries of *ITGA2B* (supplemental Table 1, available on the *Blood* Web site; see the Supplemental Materials link at the top of the online article) and *ITGB3* was amplified by polymerase chain reaction and sequenced. The disease-associated *ITGA2B* haplotype was determined by cloning and sequencing the polymerase chain reaction products.

Platelet glycoprotein analysis

Flow cytometry and immunoblotting were performed as described previously.[11,12] The activation state of αIIbβ3 was evaluated by the binding of the ligand-mimetic antibody PAC-1 (BD Biosciences) and FITC-labeled fibrinogen.[13]

Cloning, mutagenesis, and retroviral transduction

ITGA2B and *ITGB3* sequences were amplified from the patient's platelet cDNA and cloned into pcDNA3.1 (Invitrogen). T562N[13] and D723H[8] were introduced into *ITGB3* cDNA using site-directed mutagenesis. *ITGA2B* and *ITGB3* expression plasmids were cotransfected into 293T and CHO cells.

Submitted December 7, 2010; accepted March 18, 2011. Prepublished online as *Blood* First Edition paper, March 31, 2011; DOI 10.1182/blood-2010-12-323691.

The online version of this article contains a data supplement.

The publication costs of this article were defrayed in part by page charge payment. Therefore, and solely to indicate this fact, this article is hereby marked "advertisement" in accordance with 18 USC section 1734.

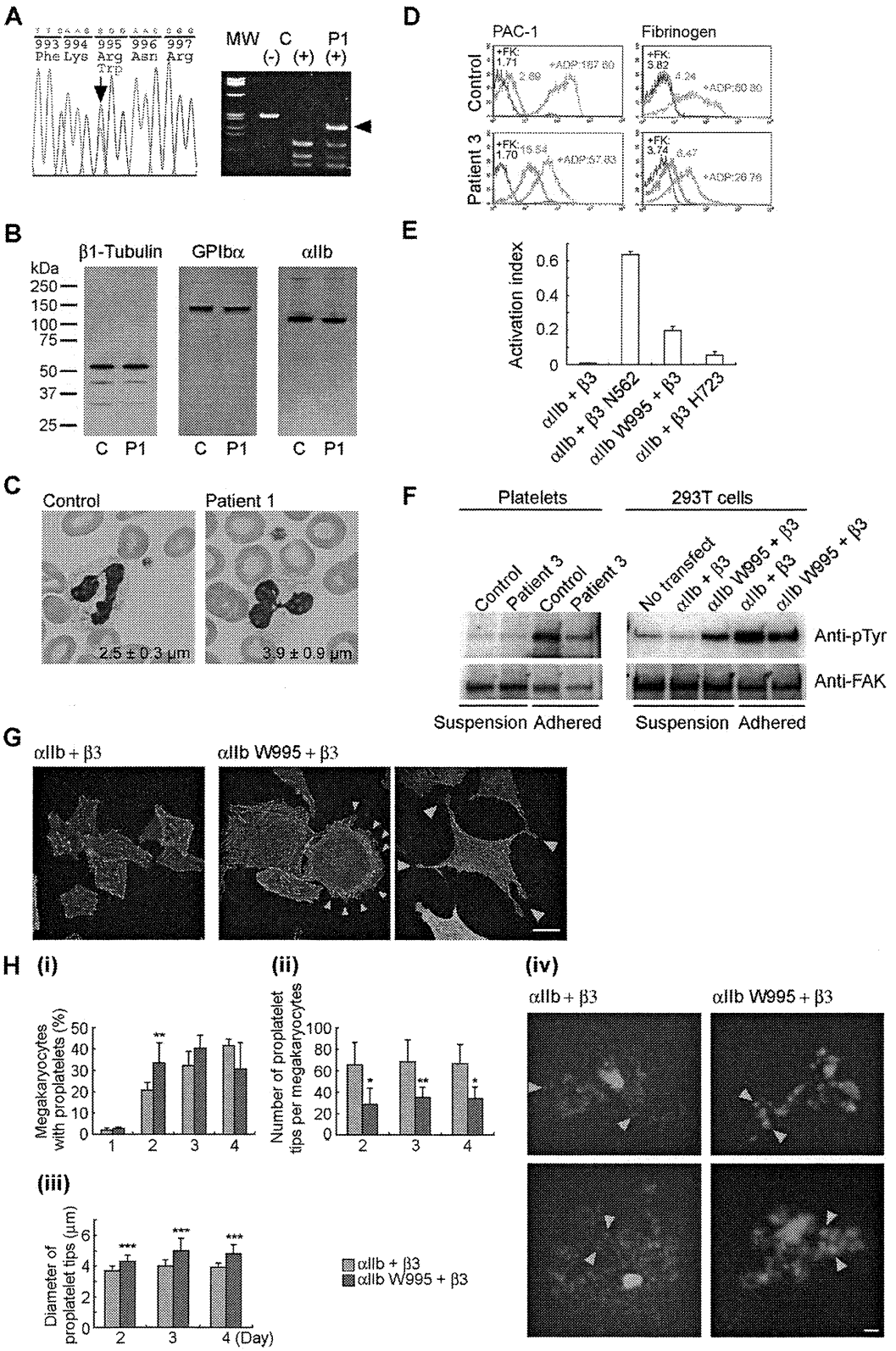

Figure 1. Platelet morphology and biochemical, genetic, and functional analyses of *ITGA2B* R995W mutation. (A; left) DNA sequence analysis of *ITGA2B*. The entire coding regions of the patients' *ITGA2B* were amplified from genomic DNA by the polymerase chain reaction, and amplified DNA fragments were subjected to direct cycle sequence analysis. A C to T transition at nucleotide 3077, changing Arg995 to Trp (R995W), was detected. Nucleotide numbering for *ITGA2B* cDNA is according to Poncz et al.[18] The arrow shows the position of the substitution. (Right) Allele-specific restriction analysis. DNA fragments amplified using primers 2Bg305/303 (supplemental Table 1) were digested with BspACI (SibEnzyme), electrophoresed on 2% agarose gels, and stained with ethidium bromide. The 3077C > T substitution abolishes a recognition site for BspACI, generating a new 231-bp band (arrowhead). The mutation was not found in 108 healthy controls or in the SNP database (www.ncbi.nlm.nih.gov/SNP). MW indicates HaeIII digest of ΦX 174 DNA; C, control; and P1, patient 1. (B) Immunoblot analysis of platelets. Triton X-100-soluble platelet lysates were separated by sodium dodecyl sulfate-polyacrylamide gel electrophoresis on 4% to 12% gradient acrylamide slab gels (Invitrogen) and electroblotted onto polyvinylidine difluoride membranes. The blots were incubated with anti-β1 tubulin antibody NB2301,[19] anti-GPIbα antibody PL524 (Takara), and anti-αIIb antibody SZ22 (Beckman-Coulter) and reacted with horseradish peroxidase-conjugated secondary antibody. The bound antibodies were visualized using an enhanced chemiluminescent substrate. C indicates control; and P1, patient 1.

Transfected cells were subjected to flow cytometry, FAK phosphorylation, and spreading assay.[13,14]

ITGA2B and *ITGB3* cDNAs were inserted upstream of internal ribosome entry site (IRES)-enhanced green fluorescent protein (EGFP) and IRES-Kusabira-Orange in the retroviral vector pGCDNsamIRES/EGFP and pGCDNsamIRES/huKO, respectively.[15,16] Each plasmid was transfected into 293gp packaging cells with a vesicular stomatitis virus G expression plasmid. Supernatants were used for the transduction of 293gpg producer cells harboring a tetracycline-inducible vesicular stomatitis virus G expression cassette,[17] and virus-bearing supernatant was harvested under tetracycline-deficient conditions.

Mouse fetal liver cells were harvested from embryonic day 13.5 embryos and cultured in Dulbecco modified Eagle medium supplemented with 10% fetal calf serum and 50 ng/mL human thrombopoietin. The next day, cells were infected with retroviruses expressing *ITGA2B* and *ITGB3* on recombinant human fibronectin fragment CH-296 (RetroNectin, Takara)-coated plates. After transduction, proplatelet formation was monitored for the next 4 days on EGFP and Kusabira-Orange double-positive megakaryocytes in suspension by inverted fluorescence microscopy. The Experimental Animal Committee of Nagoya Medical Center approved the animal studies.

Results and discussion

We searched for *ITGA2B* and *ITGB3* mutations in 27 patients with macrothrombocytopenia and identified a novel, conserved heterozygous *ITGA2B* R995W mutation in one patient (patient 1; Figure 1A). The decreased surface expression of platelet αIIbβ3 prompted us to prospectively screen its expression by flow cytometry. We detected decreased αIIbβ3 expression level (50%-70% of control) in 3 of 55 consecutive patients with macrothrombocytopenia of unknown etiology (patients 2-4 in Table 1). Immunoblotting showed a normal electrophoretic mobility of αIIb, but the total expression level relative to β1-tubulin was decreased to 0.7 (Figure 1B; Table 1). Sequence analysis identified the same heterozygous *ITGA2B* R995W mutation. In total, we identified 11 patients in 4 unrelated Japanese families. In each family, the disease-associated *ITGA2B* haplotype was unique, indicating independent occurrence (supplemental Table 2). Patients had larger platelets, approximately 30% increase of control, and moderate thrombocytopenia (Figure 1C; Table 1). These results indicate that macrothrombocytopenia shows a dominant inheritance.

Bleeding tendency was absent or mild (eg, patient 1 had undergone total colectomy without platelet transfusion). Platelet aggregation induced by adenosine diphosphate and collagen was reduced, although the bleeding time was within the normal limit (Table 1). Platelet spreading on immobilized fibrinogen was partially impaired: the number of fully spread platelets was decreased (supplemental Figure 1). These findings indicate that patients are asymptomatic or exhibit a marginal bleeding tendency and that the clinical and laboratory phenotype is distinct from Glanzmann thrombasthenia.

There was spontaneous PAC-1 binding to resting patients' platelets as well as to αIIb-W995/β3-transfected 293T cells. Although fibrinogen did not bind to platelets in whole blood, increased fibrinogen binding to the washed platelets was observed (Figure 1D; supplemental Figure 2). The activation state, quantified as an activation index in 293T cells, was higher for αIIb-W995 than for β3-H723 but was weaker than that for a strong activating mutant, β3-N562[13](Figure 1E). CD62p expression was absent on the resting platelets (supplemental Figure 2). Spontaneously phosphorylated FAK, a downstream effector of integrin signaling, was not evident in resting platelets in suspension, probably because of low expression level of abnormal αIIbβ3 receptor. However, FAK phosphorylation occurred in αIIb-W995/β3-transfected 293T cells in suspension, indicating constitutively activated αIIbβ3 (Figure 1F). These results indicate that R995W mutation changes αIIbβ3 to a constitutively, albeit partially, activated conformation, but does not induce platelet activation.

αIIb-R995 forms a salt bridge with β3-D723 in the membrane-proximal region and maintains the inactive conformation of the αIIbβ3.[20,21] Disruption of the interaction because of partially activated αIIb/β3-H723 or αIIb/β3-A723 mutants but not fully activated mutants, such as αIIb/β3-N562, was reported to cause microtubule-dependent abnormal proplatelet-like cytoplasmic extensions in megakaryocytes and CHO cells.[8,22] We found that

Figure 1. (continued) (C) Platelet morphology. Peripheral blood smears were stained with May-Grünwald-Giemsa for a normal control and patient 1 (original magnification, × 1000). The patient showed giant platelets with morphologically normal leukocytes. The number in each panel shows the mean platelet size (n = 200). Images were obtained using a BX50 microscope with a 100×/1.35 numeric aperture oil objective (Olympus). Images of the slides were acquired using a DP70 digital camera and DP manager software Version 1.2.1.107 (Olympus). (D) Activation state of platelet αIIbβ3. Washed platelets from patient 3 were resuspended in Tyrode buffer (137mM NaCl, 2.7mM KCl, 1.0mM $MgCl_2$, 3.3mM NaH_2PO_4, 3.8mM N-2-hydroxyethylpiperazine-N′-2-ethanesulfonic acid, 0.1% glucose, 0.1% bovine serum albumin, pH 7.4) and incubated with fluorescein isothiocyanate-conjugated PAC-1 or 125 μg/mL fluorescein isothiocyanate-labeled fibrinogen in the presence or absence of 10μM FK633 (αIIbβ3-specific peptidomimetic antagonist: black lines) or 10μM adenosine diphosphate (blue lines), and analyzed by flow cytometry. Numbers indicate the mean fluorescence intensity. Results are representative of 2 independent experiments. (E) Quantitation of the αIIbβ3 activation state. The activation state of αIIbβ3 was quantified as an activation index on transiently transfected 293T cells. The activation index was higher for αIIb-W995 than for β3-H723 but was weaker than for an activating mutant β3-N562. Activation index = (a − b)/(c − b), in which a is the mean fluorescence intensity of PAC-1 binding with buffer, b is the mean fluorescence intensity in the presence of FK633, and c is the mean fluorescence intensity in the presence of PT25–2 (anti-αIIbβ3 antibody, which induces the active conformation of αIIbβ3). Data are mean plus or minus SE (n = 3). (F) FAK phosphorylation. Washed platelets from patient 3 (left) or transiently transfected 293T cells (right) were incubated in suspension or seeded onto 100-μg/mL fibrinogen-coated plastic dishes for 1 hour. Cells were washed with phosphate-buffered saline and lysed with 1% Triton X-100 and 1mM sodium vanadate. FAK was immunoprecipitated from the lysates with anti-FAK antibody FAK(C903; Santa Cruz Biotechnology) and protein G-Sepharose, and phosphotyrosine was detected with the antiphosphotyrosine antibody 4G10 (Millipore). Note that 300-μg and 150-μg lysates from suspension and adhered platelets, respectively, and 200-μg lysates from suspension and adhered transfected 293T cells were used for immunoprecipitation analysis. To monitor the loading of gel lanes, the membrane was stripped and reprobed with the anti-FAK antibody FAK(A17; Santa Cruz Biotechnology). Results are representative of 2 and 3 independent experiments for platelets and transfected cells, respectively. (G) Abnormal cytoplasmic protrusions in αIIb-W995/β3-transfected CHO cells. Stably transfected CHO cells were seeded onto 100 μg/mL fibrinogen-coated glass coverslips and incubated for 2 hours at 37°C. Cells were fixed with 3.7% formaldehyde and permeabilized with 0.2% Triton X-100. Coverslips were then stained with anti-CD41a antibody HIP8 (BD Biosciences) followed by Alexa-488-labeled goat antimouse IgG (Invitrogen) and tetramethylrhodamine isothiocyanate-phalloidin (Sigma-Aldrich). Images were obtained using a confocal microscope with a Plan-Apochromat 63×/1.4 oil DIC objective lens LSM5Pascal (Carl Zeiss). Arrowheads indicate membrane ruffling (middle panel) and abnormal cytoplasmic protrusions with the bulbous tips (right panel) in αIIb-W995/β3-transfected CHO cells. Representative images from 3 independent experiments are shown. (H) Abnormal proplatelet formation in αIIb-W995/β3-transfected megakaryocytes. Mouse fetal liver-derived megakaryocytes infected with EGFP-αIIb and Kusabira-Orange-β3 retrovirus were examined in suspension cultures under an IX71 fluorescence microscope with an LCPlanFl 40×/0.60 objective lens (Olympus). (i) The percentage of megakaryocytes extending proplatelets was evaluated manually under a fluorescence microscope 1 to 4 days after infection. For each specimen, at least 100 megakaryocytes were evaluated. The number of proplatelet tips per megakaryocyte (ii) and the size of the proplatelet tips (iii) were measured on acquired images by the ImageScope software Version 10.2.2 (Aperio Technologies). At least 10 megakaryocytes were analyzed for each sample. An unpaired, 2-tailed *t* test was used to analyze data. A value of *P* less than .05 was considered statistically significant. Data are mean plus or minus SD. $*P < .05$. $**P < .01$. $***P < .0001$. (iv) Representative megakaryocytes from 3 independent experiments are shown. Note that the number of proplatelet tips/bulbous structures (arrowheads) is decreased and the size of the tips increased in αIIb-W995/β3-transfected megakaryocytes than in wild-type αIIb/β3-transfected megakaryocytes. Scale bar represents 10 μm.

Table 1. Platelet characteristics of patients with the *ITGA2B* R995W mutation

Patient	Sex	Age, y	*ITGA2B* mutation	Platelet count, $\times 10^9$/L*	Platelet size, μm†	Surface expression relative to control platelets, %‡					αIIb/β1 tubulin ratio to controls§	Duke bleeding time, minutes‖	Platelet aggregation¶			Bleeding tendency	Initial diagnosis
						αIIb	β3	αIIbβ3	GPIbα	GPIX			ADP, %	Collagen (2.0 μg/mL), %	Ristocetin (1.3 mg/mL), %		
Family 1																	
Patient 1	Male	55	R995W	65	3.9 ± 0.9	53.8	67.0	—	143.1	143.8	0.82	4.5	11 (3μM)	28	77	–	Unknown thrombocytopenia
Family 2																	
Father	Male	46	R995W	79	3.3 ± 0.9	51.3	51.4	56.5	106.7	109.8	—	—	—	—	—	–	—
Patient 2	Male	4	R995W	82	3.6 ± 1.0	54.0	58.6	61.8	138.3	134.7	0.75	5	—	—	—	Epistaxis	Congenital thrombocytopenia
Sister	Female	9	R995W	85	3.4 ± 1.0	55.6	60.6	68.4	120.0	133.1	0.71	3.5	—	—	—	–	—
Family 3																	
Mother	Female	56	R995W	80	2.8 ± 0.8	58.4	63.4	65.8	116.5	—	0.73	—				–	—
Patient 3	Female	27	R995W	74	3.5 ± 1.0	64.4	69.7	63.8	124.8	—	—	—	43 (10μM)	44	72	–	cITP
Sister	Female	24	R995W	100	3.6 ± 1.0	59.3	70.2	70.8	110.9	—	0.63	—	—	—	—	–	—
Family 4																	
Maternal grandfather	Male	58	R995W	66	3.4 ± 0.9	—	—	—	—	—	0.63	—	20 (3μM)	9	—	Hemorrhage in exodontia	—
Mother	Female	30	R995W	66	2.8 ± 0.8	56.3	62.5	57.5	127.2	112.1	0.63	2.5	—	—		Purpura, hemorrhage in exodontia	cITP
Patient 4	Female	4M	R995W	82	3.2 ± 1.0	63.3	62.9	62.3	147.7	140.5	0.63	—	23 (3μM)	11	—	–	NAITP
Brother	Male	5	R995W	122	3.1 ± 0.8	—	—	—	—	—	—	—	—	—	—	–	—
Mean ± SD				81.9 ± 16.8#	3.3 ± 0.3#	57.4 ± 4.4**	62.9 ± 5.8**	63.3 ± 5.0**	126.1 ± 14.3**	129.0 ± 14.5**	0.7 ± 0.07#						

— indicates not applicable; ADP, adenosine diphosphate; cITP, chronic immune thrombocytopenia; and NAITP, neonatal alloimmune thrombocytopenic purpura.

*Controls, 273.5 ± 60.4 ($\times 10^9$/L) (n = 1014).

†Determined by microscopic observation of 200 platelets on a stained peripheral blood smear. Controls, 2.5 ± 0.3 μm (n = 31).

‡Platelets were reacted with fluorescein isothiocyanate-labeled monoclonal antibodies against αIIb (5B12; Dako Denmark), β3 (SZ21), αIIbβ3 (P2), GPIbα (SZ2; Beckman-Coulter), or GPIX (ALMA16; BD Biosciences) and analyzed in an Epics XL flow cytometer (Beckman-Coulter). Values are expressed as percentage of mean fluorescence intensities of control platelets.

§Platelet αIIb/β1-tubulin ratio was determined by densitometric analysis of immunoblots using ImageQuant software Version 5.0 (Molecular Dynamics).

‖Normal range, 2 to 5 minutes.

¶Platelet aggregation was performed in platelet-rich plasma. Results are given as percentage maximum aggregation.

#$P < .001$, **$P < .0001$ vs controls (2-tailed t test).